

UC Davis

UC Davis Previously Published Works

Title

Modeling and simulation of earthquake soil structure interaction excited by inclined seismic waves

Permalink

<https://escholarship.org/uc/item/5wx743dg>

Authors

Wang, Hexiang
Yang, Han
Feng, Yuan
et al.

Publication Date

2021-07-01

DOI

10.1016/j.soildyn.2021.106720

Peer reviewed

Modeling and Simulation of Earthquake Soil Structure Interaction Excited by Inclined Seismic Waves

Hexiang Wang^a, Han Yang^a, Yuan Feng^a, Boris Jeremić^{a,b,*}

^a*Department of Civil and Environmental Engineering, University of California, Davis, CA, USA*

^b*Environmental and Earth Sciences Area, Lawrence Berkeley National Laboratory, Berkeley, CA, USA*

Abstract

Presented is an application of wave potential formulation (WPF) together with domain reduction method (DRM) to modeling earthquake soil structure interaction (ESSI) behavior in horizontally layered ground under inclined incident seismic waves. Wave potential formulation is used to develop a spatially varying, inclined seismic wave field from incident Primary (P) and Secondary (S) waves that propagate through layered ground. Developed seismic wave field is then used to develop effective forces for Domain Reduction Method that are then used for analyzing ESSI response of a soil structure system. Developed methodology, called WPF-DRM, is verified using analytic solution for a free field response of layered ground subjected to inclined incident waves.

Developed WPF-DRM methodology is illustrated through analysis of an ESSI response of a deeply embedded structure, a small modular reactor (SMR) subjected to incident S wave polarized in vertical plane (SV) with variation in inclinations and frequencies. Presented example highlights the

*Corresponding author

Email address: jeremic@ucdavis.edu (Boris Jeremić)

influences of incident wave inclination and frequency on ESSI response of analyzed SMR.

Keywords: earthquake soil structure interaction, deeply embedded structure, inclined incident P/SV/SH waves, layered ground, small modular reactor

1	Contents	
2	1 Introduction	4
3	2 Wave Potential Formulation – Domain Reduction Method	6
4	2.1 Wave Potential Formulation for Inclined Incident Waves in	
5	Layered Media	7
6	2.2 Domain Reduction Method	13
7	3 Illustrative Examples	15
8	3.1 Free Field Modeling and Verification	15
9	3.2 Deeply Embedded Soil-Structure Model	23
10	3.3 SMR Excited with Inclined SV Waves	25
11	3.4 SMR Excited with Variable Frequency Inclined SV Waves . .	30
12	4 Summary	37
13	5 Acknowledgments	38

14 **1. Introduction**

15 It has been recognized that during earthquakes, inclined body waves and
16 surface waves have significant influence on a dynamic response of soil struc-
17 ture interaction (SSI) systems [1–5]. For example, incident secondary (S)
18 waves, where soil/rock particles move in horizontal plane (SH), can cause
19 torsional response of structures, Similarly, incident primary (P) and sec-
20 ondary (S) waves, where particles move in vertical plane (SV), can produce
21 amplified rocking of structures, especially in near-fault regions and for struc-
22 tures with large-plan dimensions or multiple supports [6]. Earthquake Soil
23 Structure Interaction (ESSI) response due to inclined incident seismic waves
24 (i.e., P, SH and SV waves) is of significant interest in earthquake engineering.

25 The Earthquake Soil Structure Interaction problem has been studied for
26 a long time. Early work was focused on dividing an SSI problem into sim-
27 pler problems that were manageable with available methodology and tools.
28 Substructure method [7] was established to decompose the SSI problem into
29 three sub-problems:

- 30 • Free field seismic motion
- 31 • Foundation input motion, i.e. foundation wave scattering and impedance
32 function, and
- 33 • Superstructure dynamic response

34 Luco and Wong [8] studied dynamic response of SSI system under non-
35 vertically incident SH wave. SSI responses excited by in-plane wave (P, SV
36 and Rayleigh waves) were presented by Todorovska and Trifunac [9], Todor-
37 ovska [10]. Effects of site dynamic characteristics on SSI were systematically
38 investigated by Liang et al. [11, 12] for incident P, SV and SH waves.

39 Due to the limitation of substructure method and the complexity of SSI
40 problem, simplifications have been commonly made in many studies. For
41 example, underground is usually simplified as homogeneous half space or
42 a single homogeneous soil layer above the bedrock. Rigid foundation with
43 specific shape is typically assumed, in order to calculate impedance functions
44 and wave scattering. This assumption could lead to excessive scattering of
45 incident wave energy and underestimated structural response [12].

46 With increase in computer power, direct simulation of dynamic SSI using
47 finite element method (FEM), finite difference method (FDM) and boundary
48 element method (BEM) becomes feasible. Stamos and Beskos [13] studied
49 dynamic response of infinitely long tunnels in elastic or viscoelastic half-
50 space under incident seismic waves by a special direct BEM. Translational,
51 torsional and rocking response of a building SSI system excited by plane P,
52 SV and SH wave using FDM was recently studied by Gičev et al. [6], Gičev
53 et al. [14], Gičev et al. [15].

54 For direct simulation of SSI, effective input of inclined incident seismic
55 waves is of great importance. Many artificial boundary types have been de-
56 veloped by approximating the radiation condition at the finite boundaries
57 of SSI system [7, 16–18]. Using developed viscous-spring artificial boundary,
58 various SSI and rock-structure interaction (RSI) systems excited by inclined
59 incident plane waves, such as tunnels [19, 20], powerhouse [21] and under-
60 ground large scale frame structure (ULSFS) [22] were analyzed. In these
61 previous studies, inclined plane waves are generally assumed to occur in ho-
62 mogeneous ground. The only wave reflection and refraction is considered at
63 the ground surface, while multiple layers, usually present in realistic geologi-
64 cal settings, were not considered. It is noted that modeling and simulation of
65 inclined wave propagation in layered ground is more complicated because of

66 multiple reflection, refraction, reverberation and interference at both layer in-
67 terfaces and ground surface. Of interest is modeling and simulation of deeply
68 embedded structures, that extend over multiple soil layers in depth. Inclined
69 seismic wave field, propagating through a number of layers, will interact
70 with the embedded structure. Embedment and stiffness of the structure will
71 modify the seismic wave field. This effect is usually called the kinematic
72 interaction, and applies for linear elastic SSI analysis, where kinematic and
73 inertial interaction effects can be separated, superimposed [23].

74 Presented is a methodology developed to investigate influence of inclined
75 body and surface seismic wave on linear or nonlinear earthquake soil struc-
76 ture interaction (ESSI) behavior of soil-structure systems. Methodology is
77 based on Wave Potential Formulation (WPF) [24, 25] as well as Domain
78 Reduction Method (DRM) [26]. Paper is organized as follows: Brief pre-
79 sentation of Wave Potential Formulation and Domain Reduction Method is
80 given in section 2. Combined Wave Potential Formulation and Domain Re-
81 duction Method (WPF-DRM) is then verified, with select results presented
82 in section 3.1. Following that, dynamic response of a deeply embedded small
83 modular reactor (SMR) under inclined incident SV wave at different frequen-
84 cies and inclinations is analyzed and presented in sections 3.2, 3.3 and 3.4.
85 Findings are summarized in section 4.

86 **2. Wave Potential Formulation – Domain Reduction Method**

87 Presented WPF-DRM methodology consists of three main steps:

- 88 1. Analytic development of free field ground motions for a layered half
89 space, excited by an incident, inclined plane wave. Development of this
90 seismic wave field is relying on wave potential formulation in frequency-

91 wave number domain. Time domain spatially varying ground motions
92 are then synthesized through inverse Fourier transformation.

93 2. Development of the Effective Earthquake Forces, from DRM formula-
94 tion, is then performed using free field seismic motions developed in
95 the previous step.

96 3. Earthquake Soil Structure Interaction (ESSI) analysis of the soil-structure
97 system is then performed using effective earthquake forces that are ap-
98 plied to a single layer of finite elements surrounding soil-structure sys-
99 tem, so called DRM layer. The only waves that are radiated from the
100 soil-structure system and exit the DRM layer are due to oscillations of
101 the structure. These outgoing waves are absorbed by damping layers.

102 Sections 2.1 and 2.2 below provide details of Wave Potential Formulation
103 and Domain Reduction Method, respectively.

104 *2.1. Wave Potential Formulation for Inclined Incident Waves in Layered* 105 *Media*

106 Considered is an inclined wave that propagates in the layered ground, as
107 shown in Figure 1. There are n layers, with layer thickness d_m , density ρ_m ,
108 compressional wave velocity α_m and shear wave velocity β_m ($m = 1, 2, \dots, n$).
109 Focus of presented development is on inclined P and SV waves, and mode
110 conversion between them at layer boundaries. Propagation of *SH* wave is
111 simpler as there is no mode conversion, so these waves are left out of presented
112 considerations. It is noted that the wave potential formulation presented
113 below is general and also applicable to incident SH wave [25].

114 Without loss of generality, incident waves is considered to be monochro-
115 matic, single frequency, with angular frequency w and horizontal phase veloc-

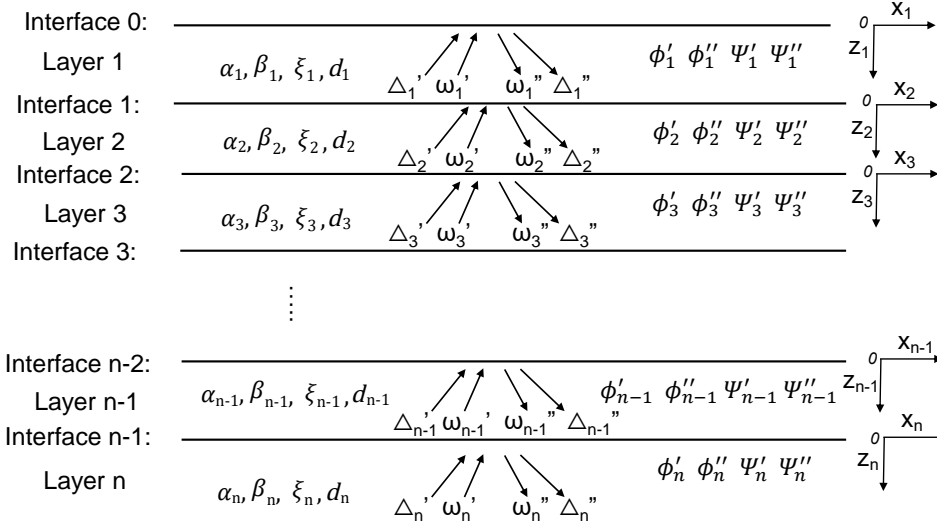


Figure 1: Layered ground and free field inclined seismic motions.

116 ity c . For incident waves with arbitrary time signal and multiple frequencies,
 117 free field motions can be Fourier synthesized from the monochromatic solu-
 118 tions.

119 According to Helmholtz decomposition theorem [27], the displacement
 120 from wave propagation modeled using Equation (1), for linear elastic material
 121 with Lamé constants λ and μ , can be expressed with P wave scalar potential
 122 ϕ and S wave vector potential Ψ .

$$\rho u_{i,tt} = \mu u_{i,jj} + (\lambda + \mu) \mu_{j,ij} \quad (1)$$

123 This is shown in Equation 2, where ϕ is the curl free part corresponding
 124 to volumetric deformation and Ψ is divergence free part corresponding to
 125 deviatoric deformation. e_{ijk} is Levi-Civita permutation symbol [27].

$$u_i = \phi_{,i} + \Psi_{k,j} e_{ijk} \quad (2)$$

126 Using this approach, the unknown displacements for the m^{th} layer are
 127 simplified into incident P wave potential magnitude ϕ'_m , reflected P wave
 128 potential magnitude ϕ''_m , incident SV wave potential magnitude Ψ'_m and
 129 reflected SV wave potential magnitude Ψ''_m , as shown in Equation 3.

$$\begin{aligned}\phi_m &= [\phi'_m e^{ik(x-\gamma_{\alpha_m}z)} + \phi''_m e^{ik(x+\gamma_{\alpha_m}z)}]e^{-i\omega t} \\ \Psi_m &= [\Psi'_m e^{ik(x-\gamma_{\beta_m}z)} + \Psi''_m e^{ik(x+\gamma_{\beta_m}z)}]e^{-i\omega t}\end{aligned}\quad (3)$$

130 In Equation 3, the horizontal wave number k is defined as $k = \omega/c$. The
 131 harmonic nature of the potential field is characterized by the time factor
 132 $e^{-i\omega t}$. The incident and reflected angles for P and SV wave are equal to
 133 $\text{arccot}\gamma_{\alpha_m}$ and $\text{arccot}\gamma_{\beta_m}$, where γ_{α_m} and γ_{β_m} are given in Equation 4.

$$\begin{aligned}\gamma_{\alpha_m} &= \begin{cases} \sqrt{(c/\alpha_m)^2 - 1} & \alpha_m \leq c \\ -i\sqrt{1 - (c/\alpha_m)^2} & \alpha_m > c \end{cases} \\ \gamma_{\beta_m} &= \begin{cases} \sqrt{(c/\beta_m)^2 - 1} & \beta_m \leq c \\ -i\sqrt{1 - (c/\beta_m)^2} & \beta_m > c \end{cases}\end{aligned}\quad (4)$$

134 Note that when compressional wave velocity α_m and/or shear wave ve-
 135 locity β_m are greater than the horizontal phase velocity c , the incidence from
 136 P or SV wave is beyond the critical angle. In that case, the incident and
 137 reflected angles for P and SV wave, γ_{α_m} and γ_{β_m} become complex num-
 138 bers. The plane wave magnitude exponentially decays along the depth. To
 139 be consistent with the original formulation by Haskell [25], dilatational wave
 140 solution Δ_m and rotational wave solution ω_m are first introduced through
 141 Equation (5).

$$\begin{aligned}\Delta &= \frac{\partial u_x}{\partial x} + \frac{\partial u_z}{\partial z} \\ \omega &= \frac{1}{2}\left(\frac{\partial u_x}{\partial z} - \frac{\partial u_z}{\partial x}\right)\end{aligned}\quad (5)$$

142 where P wave potential magnitude ϕ_m and SV wave potential magnitude
 143 Ψ_m of m -th layer are related to dilatational wave solution Δ_m and rotational
 144 wave solution ω_m through:

$$\begin{aligned}\phi_m &= -\left(\frac{\alpha_m}{w}\right)^2 \Delta_m \\ \Psi_m &= 2\left(\frac{\beta_m}{w}\right)^2 \omega_m\end{aligned}\quad (6)$$

The displacements (u_x, u_y) and inter-facial stresses (σ_{zz}, τ_{zx}) can be expressed using wave potential magnitudes ϕ and Ψ , through Equations (2) - (6). Similarly, the displacement and stress field of m^{th} layer can be calculated from the dilatational wave and rotational wave solutions Δ_m and ω_m as

$$\begin{aligned}u_x &= \left\{-ik\left(\frac{\alpha_m}{\omega}\right)^2[(\Delta'_m + \Delta''_m)\cos(k\gamma_{\alpha_m}z) - i(\Delta'_m - \Delta''_m)\sin(k\gamma_{\alpha_m}z)]\right. \\ &\quad \left.+ 2ik\gamma_{\beta_m}\left(\frac{\beta_m}{\omega}\right)^2[(\omega'_m - \omega''_m)\cos(k\gamma_{\beta_m}z) + i(\omega''_m + \omega'_m)\sin(k\gamma_{\beta_m}z)]\right\}e^{ikx}\end{aligned}\quad (7)$$

$$\begin{aligned}u_z &= \left\{ik\gamma_{\alpha_m}\left(\frac{\alpha_m}{\omega}\right)^2[(\Delta'_m - \Delta''_m)\cos(k\gamma_{\alpha_m}z) - i(\Delta''_m + \Delta'_m)\sin(k\gamma_{\alpha_m}z)]\right. \\ &\quad \left.+ 2ik\left(\frac{\beta_m}{\omega}\right)^2[(\omega'_m + \omega''_m)\cos(k\gamma_{\beta_m}z) - i(\omega'_m - \omega''_m)\sin(k\gamma_{\beta_m}z)]\right\}e^{ikx}\end{aligned}\quad (8)$$

$$\begin{aligned}\sigma_{zz} &= \rho_m \left\{\alpha_m^2 \left(1 - 2\frac{\beta_m^2}{c^2}\right) [(\Delta'_m + \Delta''_m)\cos(k\gamma_{\alpha_m}z) - i(\Delta'_m - \Delta''_m)\sin(k\gamma_{\alpha_m}z)]\right. \\ &\quad \left.+ 4\frac{\beta_m^4}{c^2} \gamma_{\beta_m} [(\omega'_m - \omega''_m)\cos(k\gamma_{\beta_m}z) - i(\omega'_m + \omega''_m)\sin(k\gamma_{\beta_m}z)]\right\}e^{ikx}\end{aligned}\quad (9)$$

$$\begin{aligned}\tau_{zx} &= 2\rho_m\beta_m^2 \left\{-\gamma_{\alpha_m}\left(\frac{\alpha_m}{c}\right)^2 [(\Delta'_m - \Delta''_m)\cos(k\gamma_{\alpha_m}z) - i(\Delta''_m + \Delta'_m)\sin(k\gamma_{\alpha_m}z)]\right. \\ &\quad \left.+ [1 - 2\left(\frac{\beta_m}{c}\right)^2] [(\omega'_m + \omega''_m)\cos(k\gamma_{\beta_m}z) - i(\omega'_m - \omega''_m)\sin(k\gamma_{\beta_m}z)]\right\}e^{ikx}\end{aligned}\quad (10)$$

145 By defining the displacement and stress solutions at m^{th} interface as col-
 146 umn vector $S^{(m)}$:

$$S^{(m)} = [\dot{u}_x(z_m = d_m)/c, \dot{u}_z(z_m = d_m)/c, \sigma_{zz}(z_m = d_m), \tau_{zx}(z_m = d_m)]^T \quad (11)$$

147 equations (7) - (10) can be reduced to the following matrix notations [25]:

$$S^{(m-1)} = \mathbf{E}_m[\Delta_m'' + \Delta_m', \Delta_m'' - \Delta_m', \omega_m'' - \omega_m', \omega_m'' + \omega_m']^T \quad (12)$$

$$S^{(m)} = \mathbf{D}_m[\Delta_m'' + \Delta_m', \Delta_m'' - \Delta_m', \omega_m'' - \omega_m', \omega_m'' + \omega_m']^T \quad (13)$$

148 where transformation matrix \mathbf{E}_m and \mathbf{D}_m are given as:

$$\mathbf{E}_m = \begin{bmatrix} -(\alpha_m/c)^2 & 0 & -\theta_m \gamma_{\beta_m} & 0 \\ 0 & -(\alpha_m/c)^2 \gamma_{\alpha_m} & 0 & \theta_m \\ -\rho_m \alpha_m^2 (\theta_m - 1) & 0 & -\rho_m c^2 \theta_m^2 \gamma_{\beta_m} & 0 \\ 0 & \rho_m \alpha_m^2 \theta_m \gamma_{\alpha_m} & 0 & -\rho_m c^2 \theta_m (\theta_m - 1) \end{bmatrix} \quad (14)$$

149 with $\theta_m = 2(\beta_m/c)^2$.

$$\mathbf{D}_m = \begin{bmatrix} -(\alpha_m/c)^2 \cos A_m & i(\alpha_m/c)^2 \sin A_m & -\theta_m \gamma_{\beta_m} \cos B_m & i\theta_m \gamma_{\beta_m} \sin B_m \\ i(\alpha_m/c)^2 \gamma_{\alpha_m} \sin A_m & -(\alpha_m/c)^2 \gamma_{\alpha_m} \cos A_m & -i\theta_m \sin B_m & \theta_m \cos B_m \\ -\rho_m \alpha_m^2 (\theta_m - 1) \cos A_m & i\rho_m \alpha_m^2 (\theta_m - 1) \sin A_m & -\rho_m c^2 \theta_m^2 \gamma_{\beta_m} \cos B_m & i\rho_m c^2 \theta_m^2 \gamma_{\beta_m} \sin B_m \\ -i\rho_m \alpha_m^2 \theta_m \gamma_{\alpha_m} \sin A_m & \rho_m \alpha_m^2 \theta_m \gamma_{\alpha_m} \cos A_m & i\rho_m c^2 \theta_m (\theta_m - 1) \sin B_m & -\rho_m c^2 \theta_m (\theta_m - 1) \cos B_m \end{bmatrix} \quad (15)$$

150 with $A_m = k\gamma_{\alpha_m} d_m$ and $B_m = k\gamma_{\beta_m} d_m$.

151 The recurrence relation between $S^{(m)}$ and $S^{(m-1)}$ then can be established
152 as shown in Equation 16, where it was used that $\mathbf{G}_m = \mathbf{D}_m \mathbf{E}_m^{-1}$.

$$S^{(m)} = \mathbf{D}_m \mathbf{E}_m^{-1} S^{(m-1)} = \mathbf{G}_m S^{(m-1)} \quad (16)$$

Recursively applying Equation 16 leads to Equation 17. Using the relation between displacement, stress response at $(m-1)^{th}$ interface $S^{(m-1)}$ and

dilatational, rotational wave solutions Δ_m, ω_m , Eq. 18 bridges the gap between the upper boundary (i.e., response at ground surface $S^{(0)}$) and lower boundary (i.e., solutions of wave incident layer Δ_n and ω_n), upon which specific boundary conditions can be imposed.

$$S^{(n-1)} = \prod_{i=1}^{n-1} \mathbf{G}_i S^{(0)} \quad (17)$$

$$S^{(0)} = \mathbf{L}[\Delta_n'' + \Delta_n', \Delta_n'' - \Delta_n', \omega_n'' - \omega_n', \omega_n'' + \omega_n']^T$$

$$\mathbf{L} = \left(\prod_{i=1}^{n-1} \mathbf{G}_i \right)^{-1} \mathbf{E}_n \quad (18)$$

153 The following boundary conditions are incorporated:

- 154 1. At n^{th} layer, the incident in-plane P and SV wave potential magnitude
 155 ϕ_n' and Ψ_n' are given as K_1 and K_2 ;
- 156 2. At the ground surface ($z = 0$), the traction is free, i.e., the third and
 157 fourth component of surface response vector $S^{(0)}$ are 0.

158 Therefore, the reflected dilatational wave magnitude and rotational wave
 159 magnitude can be solved using Equation 19, where Δ_n' is $-K_1\omega^2/\alpha_n^2$ and ω_n'
 160 is $K_2\omega^2/(2\beta_n^2)$.

$$\begin{bmatrix} \Delta_n'' \\ \omega_n'' \end{bmatrix} = \begin{bmatrix} L_{31} + L_{32} & L_{33} + L_{34} \\ L_{41} + L_{42} & L_{43} + L_{44} \end{bmatrix}^{-1} \begin{bmatrix} (L_{32} - L_{31})\Delta_n' + (L_{33} - L_{34})\omega_n' \\ (L_{42} - L_{41})\Delta_n' + (L_{43} - L_{44})\omega_n' \end{bmatrix} \quad (19)$$

161 Finally, recurrence relation, given by Equation 20

$$\begin{bmatrix} \Delta_{m-1}'' + \Delta_{m-1}' \\ \Delta_{m-1}'' - \Delta_{m-1}' \\ \omega_{m-1}'' - \omega_{m-1}' \\ \omega_{m-1}'' + \omega_{m-1}' \end{bmatrix} = \mathbf{D}_{m-1}^{-1} \mathbf{E}_m \begin{bmatrix} \Delta_m'' + \Delta_m' \\ \Delta_m'' - \Delta_m' \\ \omega_m'' - \omega_m' \\ \omega_m'' + \omega_m' \end{bmatrix} \quad (20)$$

162 can be used to trace back dilatational wave magnitude Δ_m and rotational
 163 wave magnitudes ω_m for the rest $n - 1$ layers. Based on solution for dilata-
 164 tional and rotational magnitudes for each layer, the complete displacement
 165 and stress field can be easily computed, using Equations (7) - (10).

166 In addition, viscosity can also be included with slight modification. Con-
 167 sidering Kelvin-Voigt viscoelastic material [28], viscosity can be handled with
 168 complex Lamé modulus and wave velocities as shown in Eq. 21, where ξ is
 169 the damping ratio.

$$G^* = G(1 + 2\xi i) \quad \beta_m^* \simeq \beta_m(1 + \xi i) \quad \alpha_m^* \simeq \alpha_m(1 + \xi i) \quad (21)$$

170 2.2. Domain Reduction Method

Domain Reduction Method (DRM) was originally developed for studying local topography effects on seismic motions [26, 29], while earlier work [30, 31] did note soil-structure interaction modeling as the ultimate goal. In the context of DRM, engineering system is discretized using the finite element method over interior domain Ω , within boundary Γ , containing local SSI system and reduced exterior domain Ω^+ , outside of boundary Γ . The nodes of the finite element model are then placed in three categories: interior nodes, boundary nodes between domains Ω and Ω^+ , on the boundary Γ , and exterior nodes in exterior domain Ω^+ . Corresponding nodal displacements are denoted as u_i , u_b and u_e , for interior, boundary and exterior nodes, respectively. Boundary nodes and their connected exterior nodes form a single layer of elements, called DRM layer, surrounding the interior SSI domain. The power of DRM lies in the analytical formulation of effective seismic forces

P^{eff} , given by the Equation 22.

$$P^{eff} = \begin{Bmatrix} P_i^{eff} \\ P_b^{eff} \\ P_e^{eff} \end{Bmatrix} = \begin{Bmatrix} 0 \\ -M_{be}^{\Omega^+} \ddot{u}_e^0 - K_{be}^{\Omega^+} u_e^0 \\ M_{eb}^{\Omega^+} \ddot{u}_b^0 + K_{eb}^{\Omega^+} u_b^0 \end{Bmatrix} \quad (22)$$

171 Effective seismic forces P^{eff} represent a dynamically consistent replacement
 172 for seismic forces at the hypocenter. Effective seismic forces P^{eff} are applied
 173 to the DRM layer, and produce the free field motions in a domain without
 174 local SSI system. The effective forces are developed from free field seismic
 175 motions, hence for free field finite element models, there are no seismic mo-
 176 tions leaving the system. When the structure is present, during SSI analysis
 177 the only outgoing motions are related to the radiation damping of structural
 178 motions.

179 From Eq. 22, only free field motions (u_e^0, u_b^0) at nodes of DRM layer and
 180 element mass and stiffness matrix ($M_{be}^{\Omega^+}, K_{be}^{\Omega^+}$) of DRM layer are required to
 181 calculate effective forces P^{eff} . Free field motions developed in the previous
 182 section are used in creation of the effective seismic forces as per Equation 22.

183 Presented approach, using analytic solution for free field 3 component
 184 (3C) seismic motions, that feature both body and surface waves, is more
 185 efficient and straightforward than conventional substructure method. In ad-
 186 dition to free field motions, substructure method requires to solve foundation
 187 wave scattering and impedance function, both of which are challenging tasks.
 188 It is noted that very few specific shapes of foundation, e.g., circular and rect-
 189 angular shape, embedded in simplified ground conditions have been studied
 190 using sub-structuring method [8, 32–38]. For the presented approach, free
 191 field motions under inclined incident plane waves are solved using wave po-
 192 tential formulation. Both wave scattering and dynamic SSI are automatically
 193 handled by the time domain FEM analysis that is dynamically loaded with

194 DRM effective earthquake forces. In addition, developed Wave Potential
 195 Formulation – Domain Reduction Method (WPF-DRM) offers advantages
 196 for solving locally inhomogeneous and nonlinear SSI problems under inclined
 197 seismic excitations [39–41].

198 3. Illustrative Examples

199 Presented WPF-DRM method is implemented in the Real-ESSI Simula-
 200 tor [42]. Described examples and publicly available executables for the Real
 201 ESSI sequential and parallel programs are available through Real ESSI Simu-
 202 lator web site <http://real-essi.info/>. All numerical examples presented
 203 here are analyzed using Real-ESSI Simulator version 20.01, in parallel com-
 204 puting mode, on UC Davis and Amazon Web Services parallel computers.

205 3.1. Free Field Modeling and Verification

206 Free field response of layered ground excited by an inclined incident seis-
 207 mic wave is used to illustrate and verify developed methodology. Analytic so-
 208 lutions based on Thomson-Haskell propagation matrix technique [24, 25, 43]
 209 are used for verification.

210 A finite element model for the free field, that is 300m wide and 200m
 deep, consisting of three layers, as described in Table 1, is used.

Table 1: Properties of layers: thickness d , density ρ , shear wave velocity V_s , compressional wave velocity V_p and Poisson’s ratio ν .

Layer	d [m]	ρ [kg/m^3]	V_s [m/s]	V_p [m/s]	ν
1	50	2100	500	816.5	0.2
2	100	2300	750	1403.1	0.3
3	∞	2500	1000	2081.7	0.35

211

212 It is noted that dimension of analyzed model is $300\text{m} \times 200\text{m}$, however there
213 exist additional finite elements outside this domain: DRM layer is a single
214 layer of finite elements that surround the interior domain. Beside the DRM
215 layer, there are absorbing layers consisting of multiple layers of finite elements
216 with high viscous damping. These damping layers should be thick enough to
217 absorb the outgoing waves. The thickness and damping parameters of these
218 absorbing layers are determined such that the response of exterior damp-
219 ing layer given by earthquake soil structure interaction analysis is negligible
220 compared to the inner part. A fixed boundary condition is applied to the
221 outer boundary. It is also noted that theoretically there should be no waves
222 propagating outside of the DRM layer for a free field response. Additional
223 damping layers are added in order to accommodate further, non-free field
224 model expansions and additions. Finite element size is set to 5m, and with
225 10 finite elements per wave length, this mesh can accurately propagate waves
226 of up to $f = 10\text{Hz}$, for surface soil with shear wave velocity of $V_s = 500\text{m/s}^2$,
227 as per Lysmer and Kuhlemeyer [16], Watanabe et al. [44].

228 A number of monochromatic, single frequency plane SV wave, represented
229 by a cosine function, with variable inclinations $\theta = 10^\circ, 45^\circ, 60^\circ, 80^\circ$ and vari-
230 able frequencies, $f = 1.0, 2.5, 5.0, 10.0\text{Hz}$, are applied to the layered ground
231 model using developed methodology. The incident SV wave magnitude from
232 the depth is 0.06m and is kept the same for all the analyzed cases. It is noted
233 that inclination angle θ is measured between a wave propagation direction
234 vector and vertical axes. The wave inclination θ depends on many factors,
235 e.g., source focal mechanism and radiation pattern, wave propagation path
236 and local site geology and topography. The typical range of inclination is
237 $0^\circ \sim 40^\circ$ [45, 46]. For example, Tabatabaie et al. [45] estimated that the in-
238 cidence angle of shear waves at the SMART-1 array site is around 20 degrees

239 using the recorded motions from 1981 Taiwan earthquake. For far-field, flat
240 engineering site with large impedance contrast (e.g., soft soil overlying stiff
241 bedrock), the assumption of vertical wave propagation can be adopted due to
242 very small inclination of incident seismic waves. However, for near-field, hard
243 rock site with low impedance contrast or engineering site with significant to-
244 pography, incidence angle of seismic waves tends to be large and inclined
245 wave propagation should be carefully modeled.

246 Free field motions are developed and introduced into the model through
247 WPF-DRM. Figure 2 shows snapshots of wave displacements in the model,
248 for a wave frequency of $f = 5\text{Hz}$, for different input plane wave inclinations,
249 $\theta = 10^\circ, 45^\circ, 60^\circ, 80^\circ$. Figure 3 shows snapshots of wave displacements in the
250 model, for a wave that is inclined at $\theta = 60^\circ$, for variable input plane wave
251 frequencies $f = 1.0, 2.5, 5.0, 10.0\text{Hz}$.

252 Few notes are in order upon visual inspection of results in Figures 2 and
253 3. The outgoing waves in exterior region, outside DRM layer, are negligibly
254 small, almost zero for all the cases. This is indeed expected, as it follows
255 from the theory of the domain reduction method [26, 29], whereby the so
256 called residual field (w_e) should be non-existent for free field motions, that
257 were used to develop effective DRM forces.

258 Comparing free field responses for SV wave with different incident angles,
259 Figure 2, the $\theta = 10^\circ$ case behaves very similar to 1D vertically propagat-
260 ing motion field that is commonly used in engineering practice. It is noted,
261 however that there are still vertical motions at the surface due to such al-
262 most vertical SV wave interacting with the free surface. For cases where
263 wave inclination is more significant, for $\theta = 45^\circ$ and $\theta = 60^\circ$, significant sur-
264 face motions are observed, with pronounced vertical and horizontal motions.
265 When the incident wave inclination is $\theta = 80^\circ$, seismic wave propagates al-

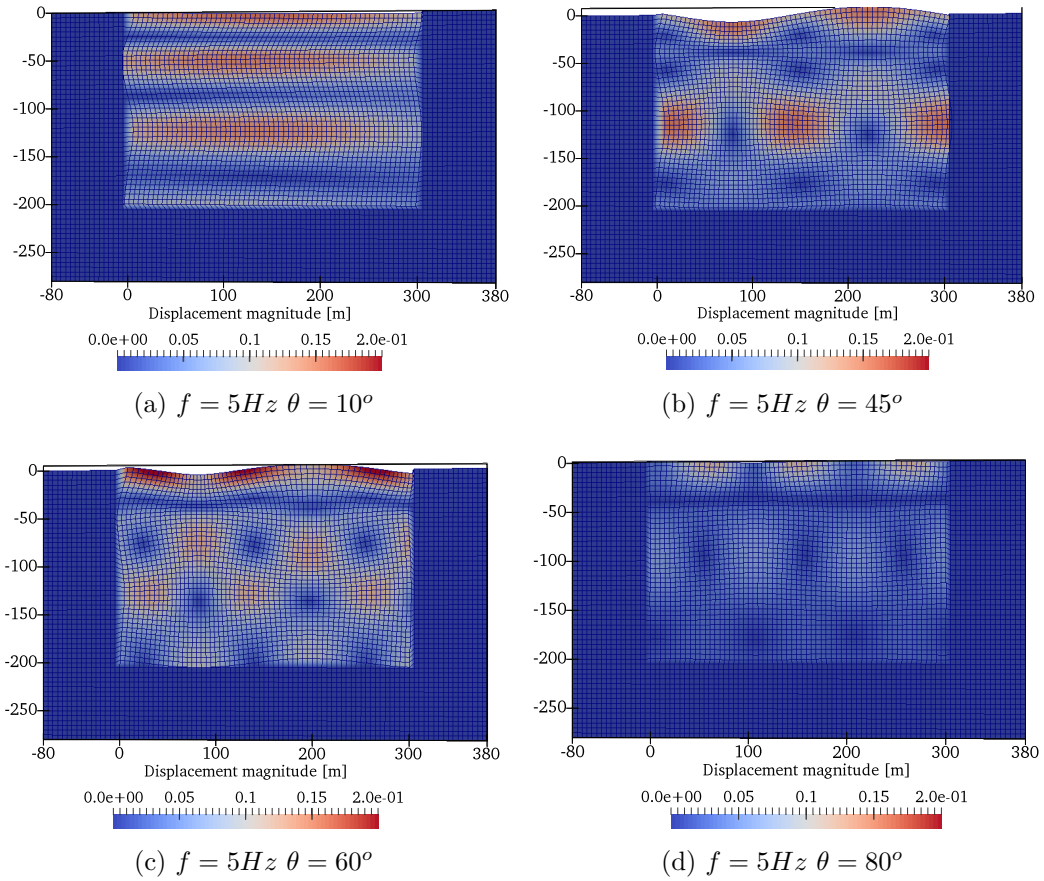


Figure 2: Displacement magnitudes for a free field response under incident SV wave, frequency $f = 5Hz$, with different incident wave inclinations: (a) $\theta = 10^\circ$ (b) $\theta = 45^\circ$ (c) $\theta = 60^\circ$ (d) incident angle $\theta = 80^\circ$.

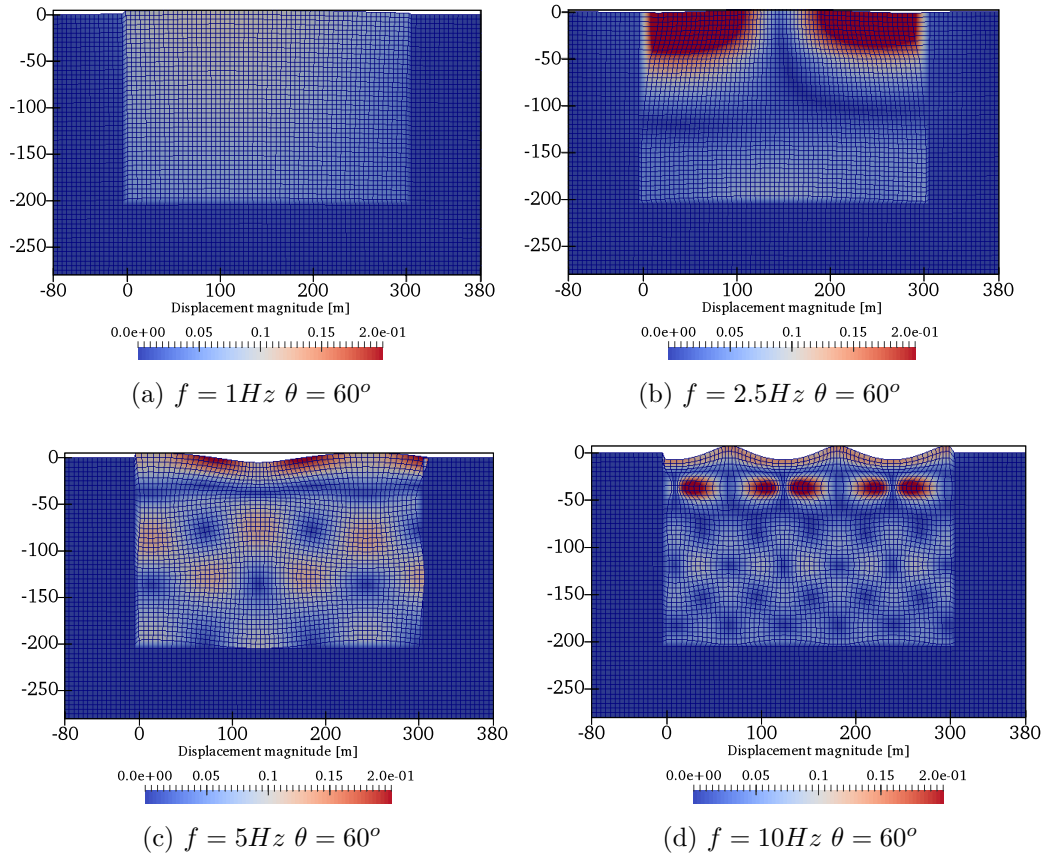


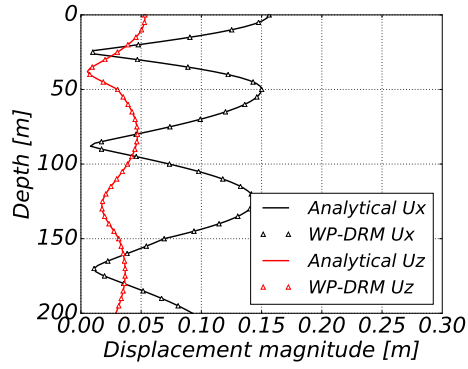
Figure 3: Displacement magnitudes for a free field response under incident SV wave at an angle of $\theta = 60^\circ$, with different frequencies: (a) $f = 1.0Hz$ (b) $f = 2.5Hz$ (c) $f = 5.0Hz$ (d) $f = 10.0Hz$.

266 most horizontally without generating significant surface motions. It is also
267 noted that the displacement magnitude of the seismic wave field for wave
268 inclination case $\theta = 80^\circ$ is much smaller than for the other cases. This is
269 reasonable considering the site amplification for other free field cases comes,
270 in part, from the impedance contrast of vertical wave propagation.

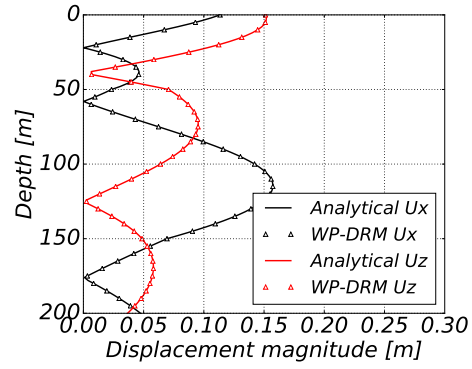
271 Results, snapshots of displacement field magnitudes for wave fields of
272 different frequencies are shown in Figure 3 for seismic motion inclined SV
273 wave field at $\theta = 60^\circ$. It is noted that layer boundaries, impedance con-
274 trasts, are at -50m , and at -150m . Those layer boundaries can be visually
275 identified from distribution of waves through model depth with positive and
276 negative interference reflected and refracted waves within different layers of
277 the domain.

278 Figures 4 and 5 compare simulated free field horizontal and vertical dis-
279 placement magnitudes against corresponding analytical solutions along the
280 depth. It is noted that acceleration magnitudes can be obtained by multi-
281 plying displacement magnitudes with w^2 . Very good agreement is observed
282 between results given by WPF-DRM simulation and analytical solutions.
283 Several interesting observations can also be made:

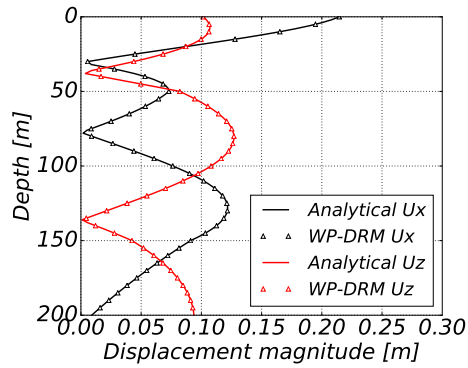
- 284 1. Along with the increase in frequencies, the vertical wave length becomes
285 shorter, and that results in more wave interferences along the depth.
- 286 2. The existence of layers and interfaces at $z = -50\text{m}$ and $z = -150\text{m}$
287 complicates the spatial variation of wave field along the depth, espe-
288 cially for higher frequencies, $f = 5Hz$ and $10Hz$. The response curves
289 at depths $0 \sim 50\text{m}$ and $50 \sim 150\text{m}$ are quite different in both amplitude
290 and variation pattern.
- 291 3. From Fig. 4, it can be seen that inclination angle of input SV wave also



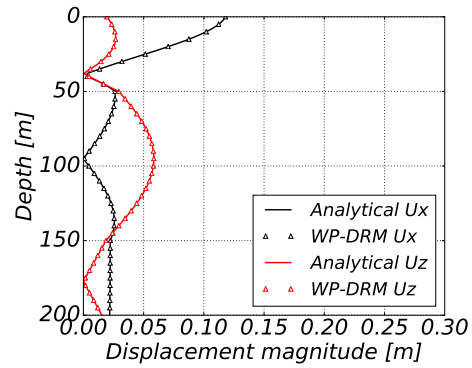
(a) $f = 5Hz$ $\theta = 10^\circ$



(b) $f = 5Hz$ $\theta = 45^\circ$

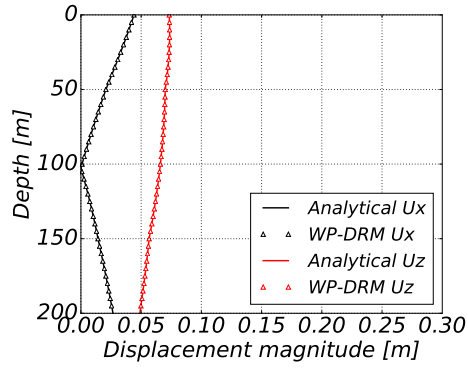


(c) $f = 5Hz$ $\theta = 60^\circ$

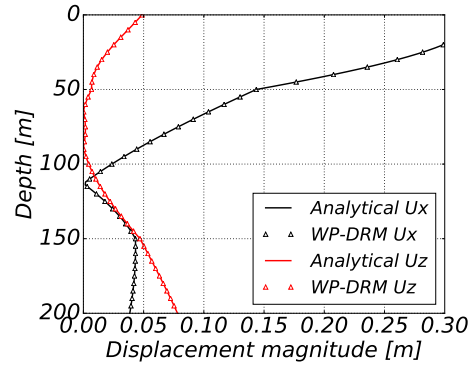


(d) $f = 5Hz$ $\theta = 80^\circ$

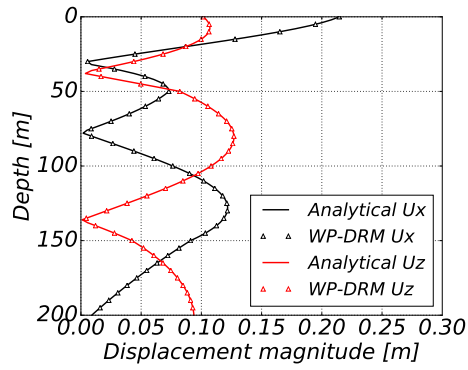
Figure 4: Verification of free field modeling under incident SV wave with different incident angles θ : (a) $\theta = 10^\circ$, (b) $\theta = 45^\circ$, (c) $\theta = 60^\circ$ (d) $\theta = 80^\circ$.



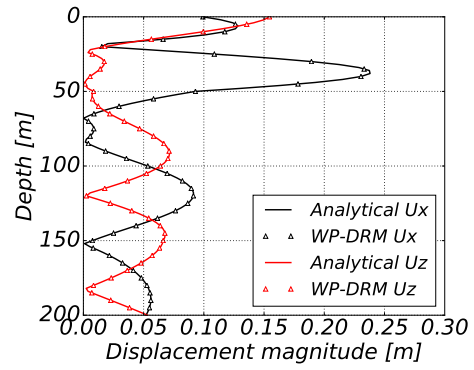
(a) $f = 1Hz$ $\theta = 60^\circ$



(b) $f = 2.5Hz$ $\theta = 60^\circ$



(c) $f = 5Hz$ $\theta = 60^\circ$



(d) $f = 10Hz$ $\theta = 60^\circ$

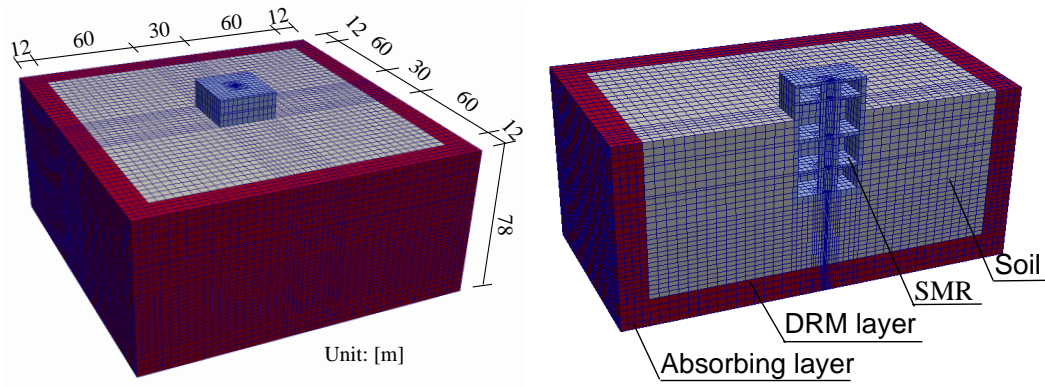
Figure 5: Verification of free field modeling under incident SV wave with different frequencies f : (a) $f = 1.0Hz$, (b) $f = 2.5Hz$, (c) $f = 5.0Hz$, (d) $f = 10.0Hz$.

292 plays a crucial role in the interference characteristic of inclined wave
293 field. Periodic peaks and troughs shown in the case of 10° inclination
294 are typical interference characteristics of 1D homogeneous, vertically
295 propagating wave field. However, the interference characteristics given
296 by other wave inclinations show significant differences. These different
297 variation patterns along the depth, that might not make much differ-
298 ence for shallow founded surface structures, can result in very different
299 seismic response for deeply embedded structures.

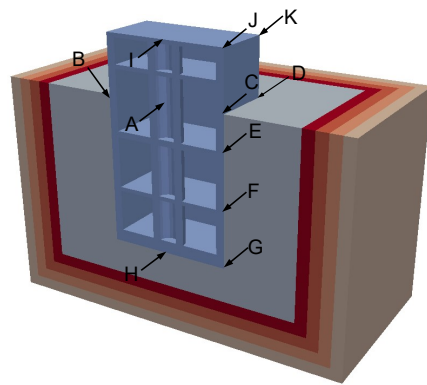
300 *3.2. Deeply Embedded Soil-Structure Model*

301 Deeply embedded structural model, a model of a Small Modular Reac-
302 tor (SMR) is analyzed and used to illustrate developed methodology. The
303 FEM model of an SMR structure embedded in layered ground is shown in
304 Figure 6(a). The embedment depth is 36m, while the height of SMR struc-
305 ture above ground is 14m. The structure width is 30m and the whole model
306 width of SSI system is 150m. It is noted that the lateral extent of soil domain
307 should be large enough such that the outgoing waves passing through DRM
308 layer are insignificant. These waves can then be damped out through the
309 absorbing layer and would have negligible influence on the dynamic response
310 of SMR. Key factors to determine the model width of SSI system include
311 structural width, intensity of seismic excitations, etc. Detailed discussions
312 regarding the required lateral extent of soil domain for dynamic SSI analysis
313 can be found in Sharma et al. [47]. Eleven representative points, point A
314 to point K in Figure 6(b), are selected to monitor the dynamic response of
315 SMR. The layered ground parameters are the same as those used in free field
316 study given in Table 1.

To proper model wave propagation, the finite element size and time step should be carefully controlled to reduce discretization errors. For linear dis-



(a) FEM model of SSI system with embedded SMR



(b) Representative points configuration

Figure 6: FEM model of embedded SMR and representative points.

placement approximation within finite element, in this case eight-node brick elements, at least 10 nodes per wavelength should be used [44]. The time step length Δt is limited by Courant-Friedrichs-Lewy condition [48] for stability. In addition, following requirement needs to be met to accurately capture the propagation of wave front [49], where Δh is the mesh size and v is the highest wave velocity.

$$\Delta t < \frac{\Delta h}{v} \quad (23)$$

317 In this study, eight-node brick element with 4m mesh size is used for
 318 spatial discretization. The maximum frequency the model can propagate is
 319 about $12.5Hz$ considering the minimum elastic shear wave velocity $500m/s$.
 320 Time step is chosen as $\Delta t = 0.005s$. Newmark time integration method [50]
 321 is used with Newmark parameters $\gamma = 0.505$ and $\beta = 0.25(0.5 + \gamma)^2$. Since
 322 parameter $\gamma > 0.5$, a small amount of numerical, algorithmic damping is
 323 introduced to damp out unrealistic high frequency responses from spatial
 324 discretization [51]. See Yang et al. [52, 53] for more information about the
 325 proper selection of Newmark parameters for dynamic analysis. Gradually
 326 increasing Rayleigh damping (7%, 15% and 30%) is assigned to the inner,
 327 middle and exterior part of the absorbing layers, outside of the DRM layer,
 328 to prevent reflection of radiated outgoing waves [49, 54]. These damping
 329 values are determined such that after dynamic SSI analysis the response of
 330 the exterior absorbing layer is negligible compared to the inner part.

331 3.3. SMR Excited with Inclined SV Waves

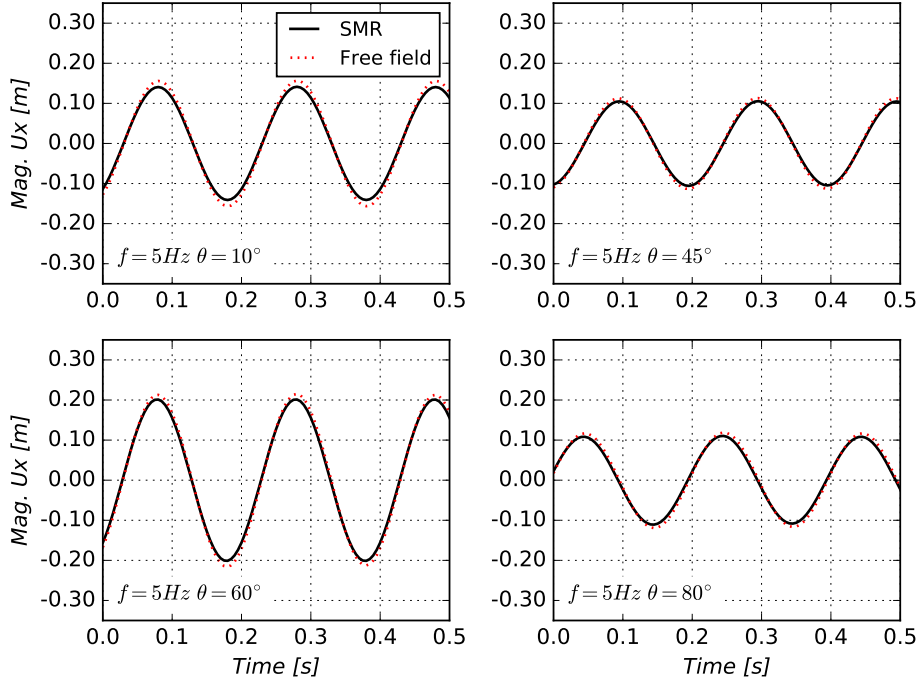
332 Deeply embedded SMR structure is excited with inclined plane waves, at
 333 inclination angles of $\theta = 10^\circ, 45^\circ, 60^\circ$ and 80° . Seismic wave frequency used
 334 for this set of numerical test was set at $f = 5Hz$. As described in table 1 on
 335 page 15, shear wave velocities of top 50m layer is $V_s = 500m/s$ while the lower

336 layer is 100m thick and has a shear wave velocity of $V_s = 750\text{m/s}$. Due to
337 presence of layers, seismic wave field close to the surface is made up Rayleigh
338 and Stoneley waves [55, 56]. It might thus be difficult to separate influence
339 of these different surface waves the response of the SMR. For example, in
340 Figure 2 on page 18, that shows displacement magnitudes at certain time,
341 for different inclination of incident plane wave, Stoneley wave is apparent
342 close to depth of 50m. In addition, Rayleigh wave is also apparent close to
343 free field surface. Those wave fields, when applied to the SMR SSI system,
344 produce response, at location of point A¹ on SMR structure, as shown in
345 Figures 7 and 8.

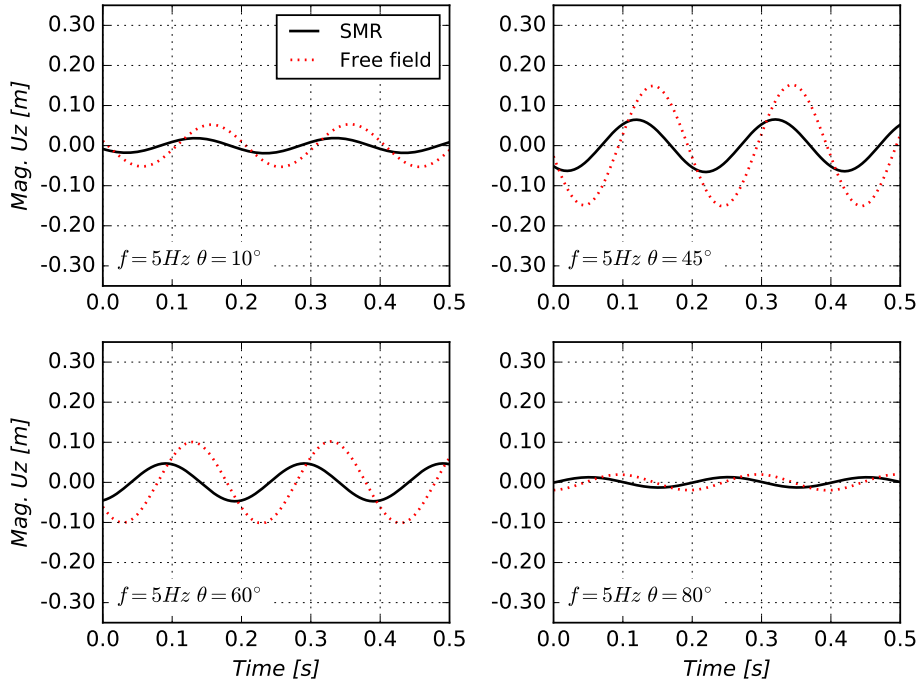
346 It is noted that corresponding free field motions at the same location are
347 also plotted for comparison. Variations of displacement magnitudes caused
348 by different inclinations of incident SV wave are quite noticeable for vertical
349 displacements and accelerations, while influence on horizontal displacements
350 and accelerations is much less significant. The reduction of vertical displace-
351 ment and accelerations that is observed in all the four cases, is consistent with
352 the concept of “base averaging”, “ironing out” of seismic motions by Housner
353 [57]. The most significant reduction occurs for the case of incident wave at
354 an angle $\theta = 45^\circ$ while little reduction is seen in the case of $\theta = 80^\circ$.

355 The deformed shapes of SMR at $t = 0.4\text{s}$ for four scenarios are shown in
356 Figure 9. In the cases of seismic waves at inclinations $\theta = 45^\circ$ and $\theta = 60^\circ$,
357 rocking responses of SMR are quite evident when compared with the cases
358 of almost vertical wave propagation ($\theta = 10^\circ$) and almost horizontal wave
359 propagation ($\theta = 80^\circ$).

¹Location of point A is in the middle of SMR structure, where center of the free field model would be, please see Figure 6 on page 24.

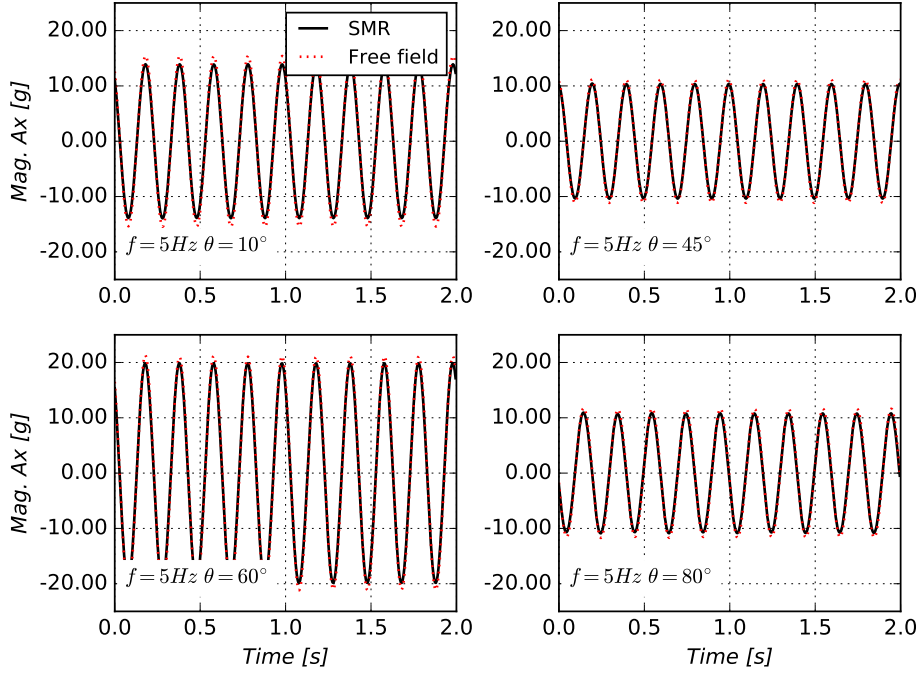


(a) Horizontal displacement

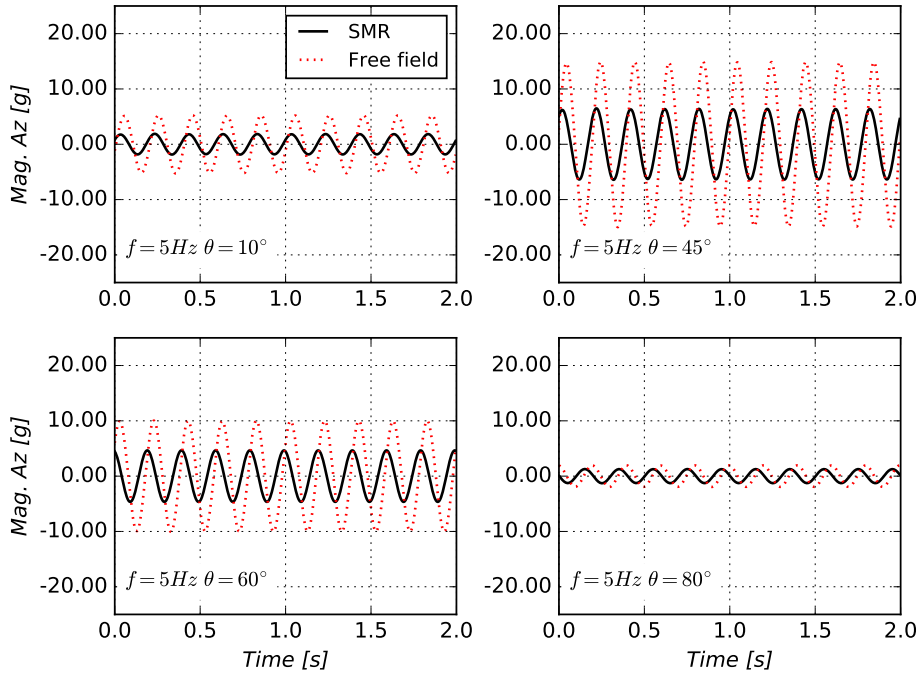


(b) Vertical displacement

Figure 7: Displacement response of point A within embedded SMR, excited by an inclined SV wave with $f = 5\text{ Hz}$ and different inclination angles, $\theta = 10^\circ, 45^\circ, 60^\circ$ and 80° : (a) horizontal displacement (b) vertical displacement.



(a) Horizontal acceleration



(b) Vertical acceleration

Figure 8: Acceleration response of point A within embedded SMR, excited by an inclined SV wave with $f = 5\text{Hz}$ and different inclination angles, $\theta = 10^\circ, 45^\circ, 60^\circ$ and 80° : (a) horizontal acceleration (b) vertical acceleration.

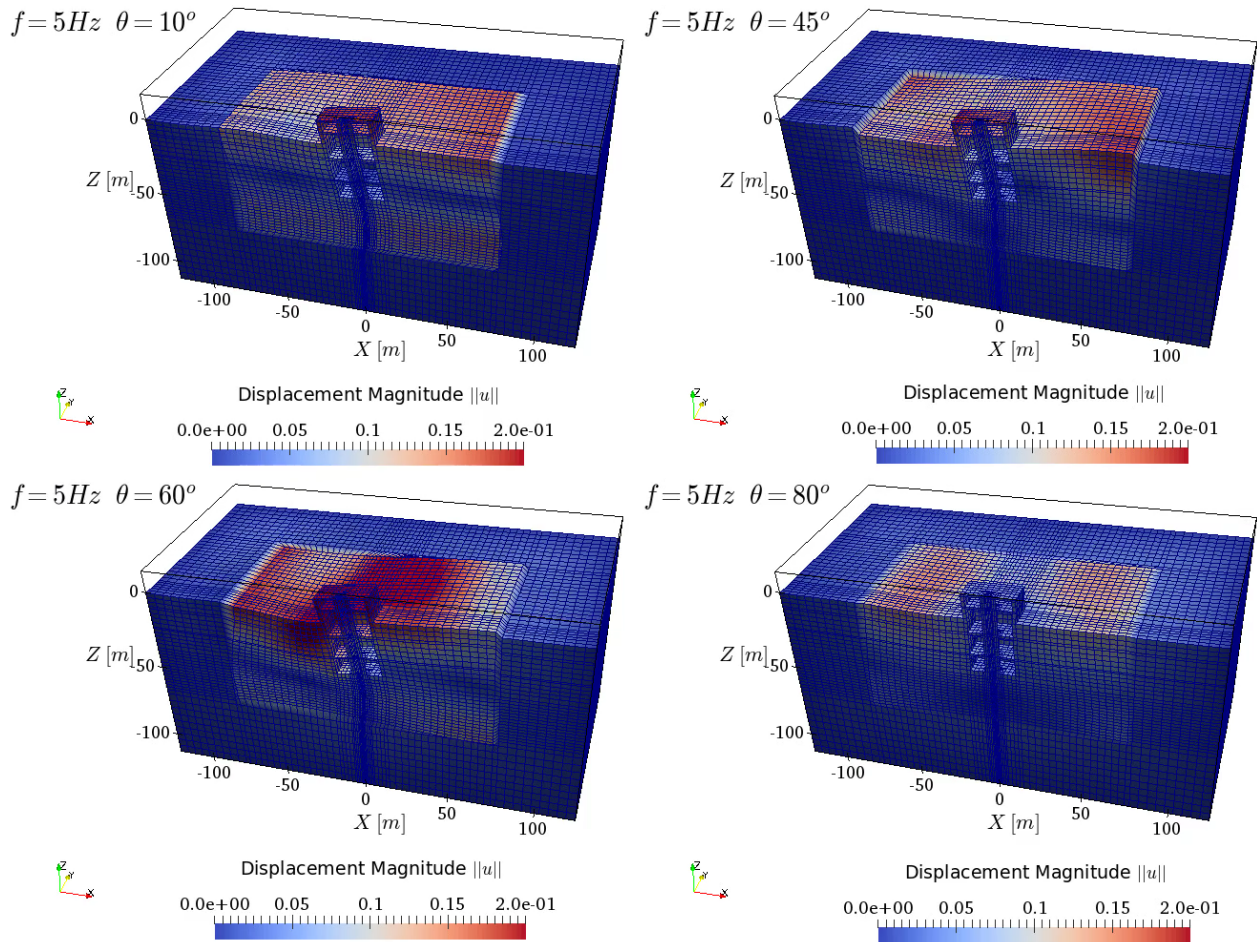


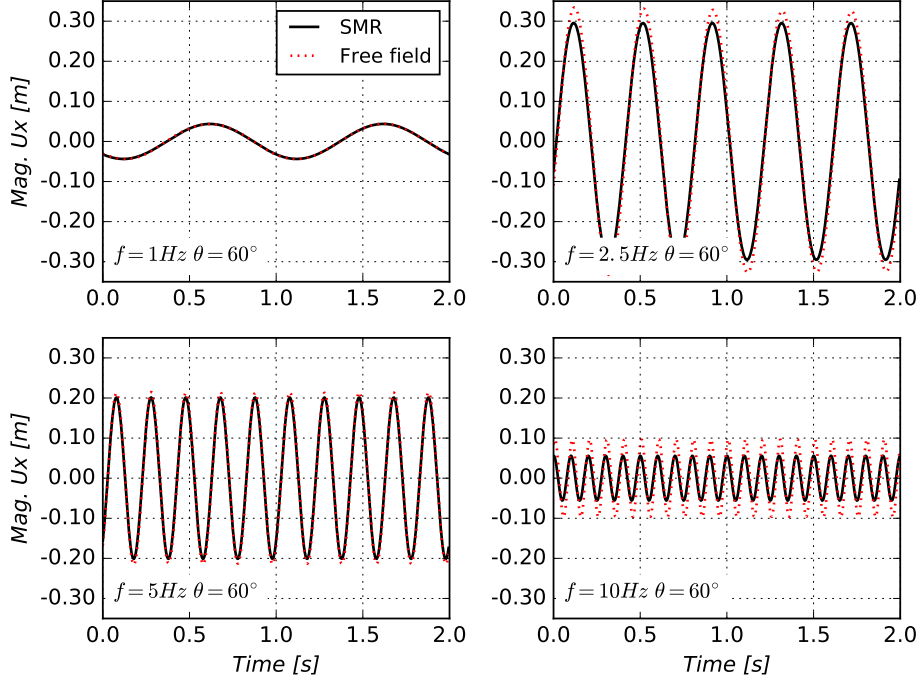
Figure 9: The deformed shapes of SMR at $t = 0.4s$ for incident SV wave at different inclinations $\theta = 10^\circ, 45^\circ, 60^\circ$ and 80° .

360 *3.4. SMR Excited with Variable Frequency Inclined SV Waves*

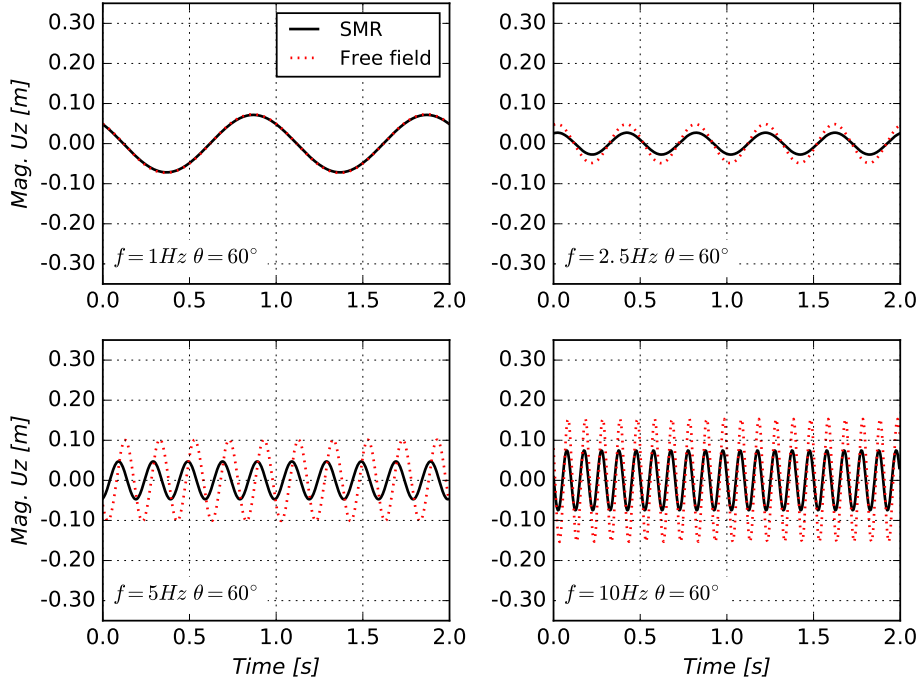
361 Keeping incidence angle constant, at $\theta = 60^\circ$, dynamic responses of an
362 SMR under different frequencies of SV wave ($f = 1Hz, 2.5Hz, 5Hz$ and $10Hz$)
363 is investigated next. Figures 10 and 11, show displacement and acceleration
364 responses at point A of SMR model.

365 It is noted that, again, free field response at the location of point A is
366 also shown for comparison purposes. Significantly variation in displacement
367 and acceleration responses are produced by incident SV wave at different fre-
368 quencies. The largest horizontal displacement magnitude 0.30m is observed
369 for the case of frequency of $f = 2.5Hz$ while the smallest horizontal magni-
370 tude of 0.047m for $f = 1Hz$. The vertical displacement responses varies from
371 0.02m for $f = 2.5Hz$ to 0.085m for $f = 10Hz$. SSI effects are almost negligi-
372 ble in the case of $f = 1Hz$ due to long horizontal wave length of 1154m. This
373 observation follows similar observation made many years ago by Housner [57]
374 for large stiff buildings. Both horizontal and vertical displacements of SMR
375 overlap with corresponding free field response for $f = 1Hz$. Along with the
376 increase of incident frequency, SSI effects become more significant, especially
377 for the vertical components of displacement and acceleration. In the cases of
378 $f = 2.5Hz$ and $f = 5Hz$, horizontal response of SMR is still very close to its
379 free field counterpart, for both displacements and accelerations, however the
380 reduction of vertical response of SMR becomes more significant for frequency
381 of $f = 5Hz$, For relatively high frequency of $f = 10Hz$, both horizontal and
382 vertical response of SMR are significantly different from free field modeling
383 in both displacements and accelerations.

384 The spatial variation of displacements at the surface of free field model
385 and at the same location within SMR model, along the horizontal line through
386 SMR (i.e. $x \in [-75m, 75m], y = 0m, z = 0m$), at $t = 3.5s$ are shown in Fig-

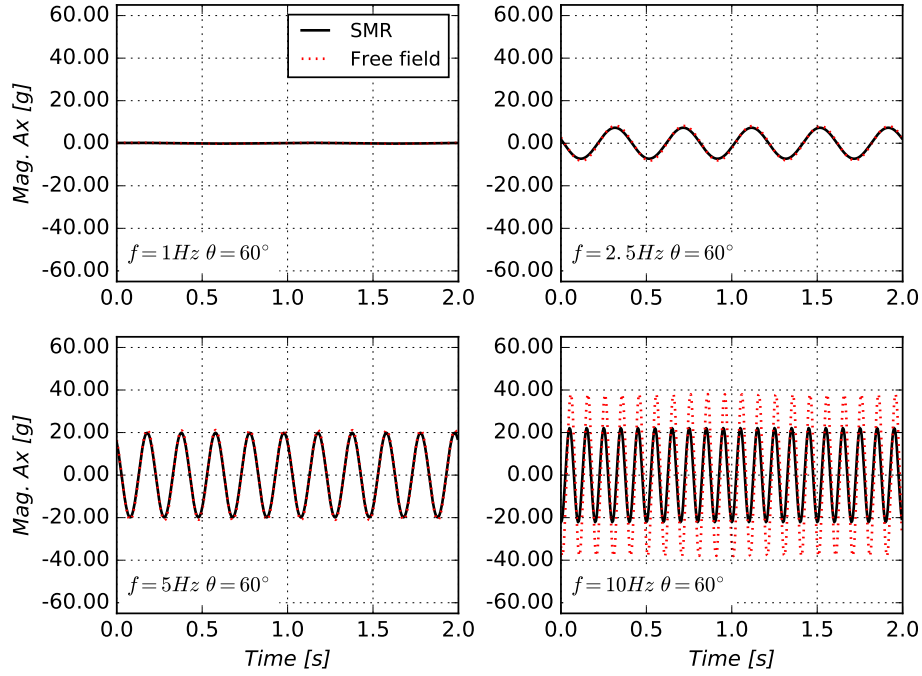


(a) Horizontal displacement

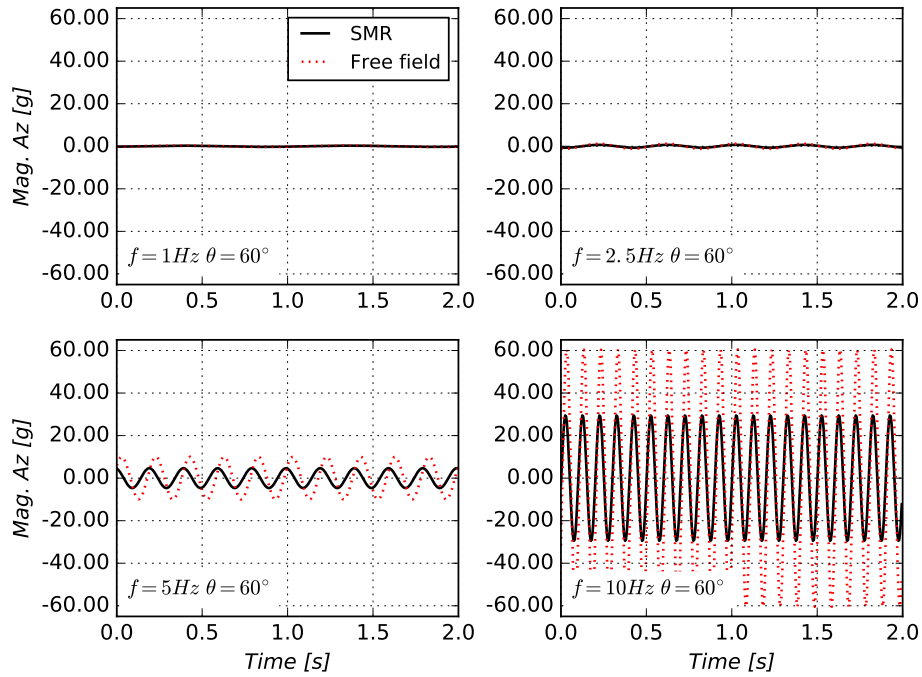


(b) Vertical displacement

Figure 10: Displacement response of point A for scenarios with different frequencies of incident SV wave: (a) Horizontal displacement (b) Vertical displacement.



(a) Horizontal acceleration



(b) Vertical acceleration

Figure 11: Acceleration response of point A for scenarios with different frequencies of incident SV wave: (a) Horizontal acceleration (b) Vertical acceleration.

387 ure 12. It is noted that SMR structure occupies space for $x \in [-15m, 15m]$,
 388 where flat trace of displacements within a stiff structure is observed. The

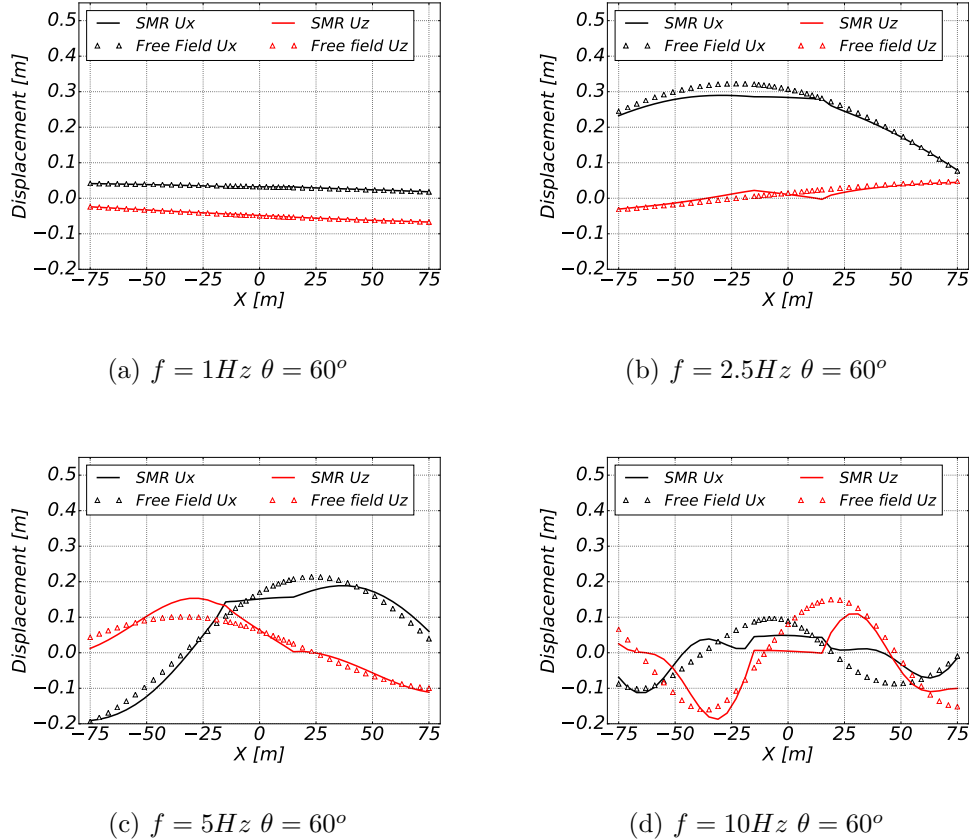


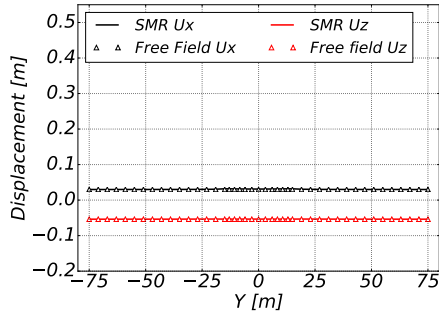
Figure 12: Spatial variation of displacement along the horizontal axis at $t = 3.5s$ for different incident wave frequencies (a) $f = 1Hz$ (b) $f = 2.5Hz$ (c) $f = 5Hz$ (d) $f = 10Hz$.

388

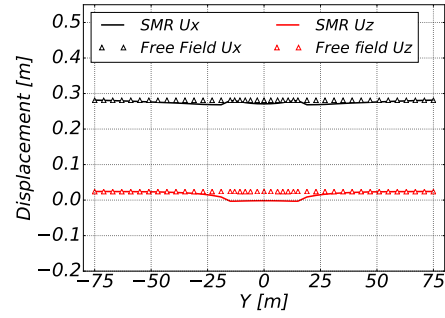
389 base slab averaging is observed for higher frequency, shorter wave length
 390 cases of $f = 5Hz$ and $f = 10Hz$, while it is almost negligible for incident
 391 waves at frequencies of $f = 1Hz$ or $f = 2.5Hz$ due to the wavelength being
 392 longer than object size for those low frequencies.

393 Similar spatial variation of displacement along the transverse axis (i.e.

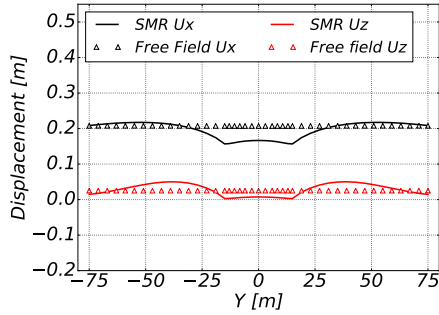
$x = 0m, y \in [-75m, 75m], z = 0m$) is shown in Figure 13. Since the inci-



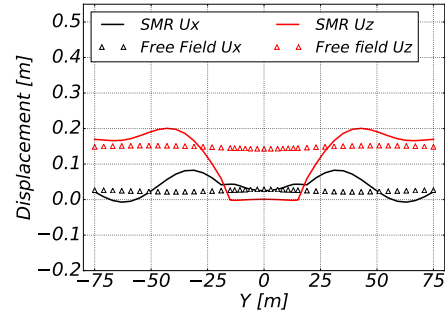
(a) $f = 1Hz \theta = 60^\circ$



(b) $f = 2.5Hz \theta = 60^\circ$



(c) $f = 5Hz \theta = 60^\circ$



(d) $f = 10Hz \theta = 60^\circ$

Figure 13: Spatial variation of displacement along the transverse axis at $t = 3.5s$ for different incident wave frequency (a) $f = 1Hz$ (b) $f = 2.5Hz$ (c) $f = 5Hz$ (d) $f = 10Hz$.

394

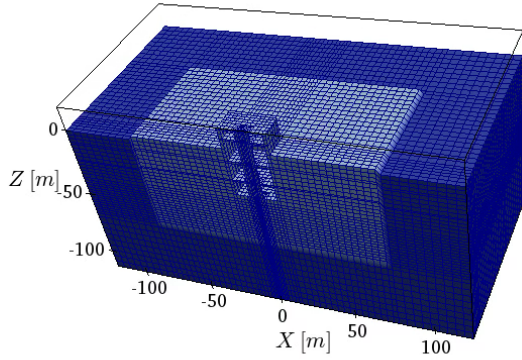
395 dent SV wave propagates within the XZ plane, uniform distribution of both
 396 horizontal and vertical free field response along the transverse axis (Y axis)
 397 is expected and presented in Figure 13. However, the existence of SMR al-
 398 ters the original uniform distribution, and a wave field in this, out plane of
 399 polarization direction. Significant wave field disturbance effects can be ob-
 400 served within the structure part ($y \in [-15m, 15m]$) in the cases of medium

401 ($f = 5Hz$) to high frequency ($f = 10Hz$). In other words, 3C dynamic re-
402 sponse of soils surrounding the structure has been induced from 2C excitation
403 by an SV wave due to SSI and transverse wave field disturbance effects.

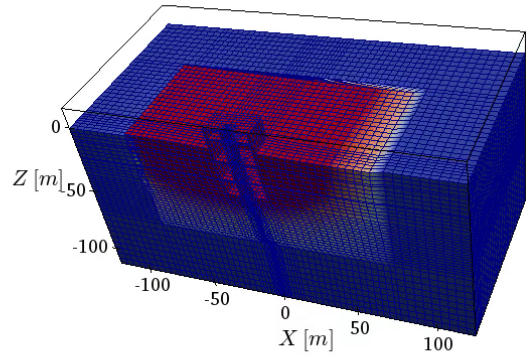
404 Another important observation from Fig. 13(d) is that, although the
405 reduction of displacement amplitude is observed within the structure, in lo-
406 cations where $y \in [-15m, 15m]$, near field motions close to the structure can
407 be amplified, for example, motion within region $y \in \pm[25m, 50m]$ in this case.
408 This implies that there are potentially significant structure-soil-structure dy-
409 namic effects for closely spaced structures.

410 The deformed shapes of SMR for four frequency scenarios at $t = 0.3s$ with
411 different frequencies are shown in Fig. 14. The aforementioned wave field
412 disturbance effects are clearly visible for the low wave length, high frequency
413 case of $f = 10Hz$. The existence of local structure has significantly altered
414 the near field seismic wave due to strong SSI effect, since wave lengths are
415 shorter than the dominant dimension of the structure.

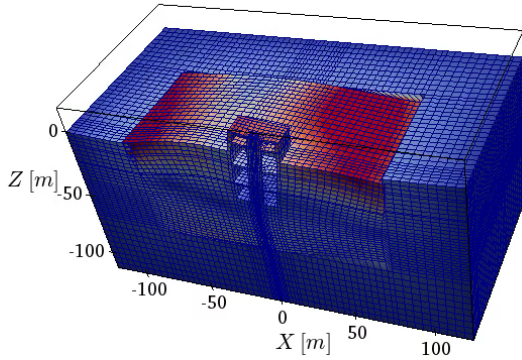
$f = 1Hz$



$f = 2.5Hz$



$f = 5Hz$



$f = 10Hz$

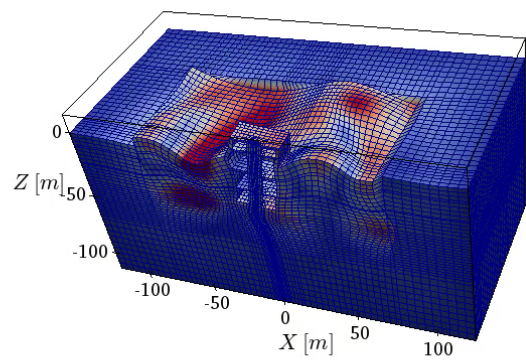


Figure 14: The deformed shapes of SMR at $t = 0.3s$ for four scenarios.

416 4. Summary

417 Presented was Wave-Potential-Formulation (WPF) – Domain Reduction
418 Method (DRM) approach, called WPF-DRM, for solving Earthquake Soil
419 Structure Interaction (ESSI) problems in layered ground excited by inclined
420 incident seismic waves. Developed WPF-DRM methodology removes a need
421 for many simplifying assumptions that are used in ESSI analysis, for example
422 rigid foundation and homogeneous ground assumption. In addition, difficul-
423 ties of solving for foundation wave scattering and impedance function are
424 also circumvented. Most importantly, developed WPF-DRM method can be
425 used with nonlinear, inelastic soil, interface and structural material behavior.
426 WPF-DRM is verified through recoverability test (i.e., resumption behavior)
427 of free field motions in a layered ground under incident SV waves.

428 Application of WPF-DRM is illustrated by analyzing a problems of an
429 ESSI response of a deeply embedded structure, a small modular reactor
430 (SMR). Focus was on analyzing influence of a number of differently inclined
431 plane waves and a number of different wave frequencies, wave lengths. It
432 is noted that free field responses for incident SV waves of varying frequen-
433 cies and inclinations show significant differences between free field and SSI.
434 For free field response, surface rolling movement pattern, Rayleigh waves are
435 captured. This is different from typically assumed, vertically propagating
436 wave field, and differences in SSI behavior are quite significant especially for
437 medium and high frequency inclined incident wave. For sensitivity study,
438 a monochromatic SSI response of SMR under incident SV wave with dif-
439 ferent frequencies and inclinations is analyzed. It is found that SSI effects
440 are more prominent considering seismic motions with non-vertical incidence
441 and relatively high frequency, low wave lengths. The vertical structural re-
442 sponse is significantly influenced by the inclinations of incident wave. The

443 vertical structure response can vary by a factor of 7 for different inclinations.
444 Compared with almost vertical wave field ($\theta = 10^\circ$ inclination) and almost
445 horizontal wave field ($\theta = 80^\circ$ inclination), more significant structural rock-
446 ing response is observed in the cases of inclination $\theta = 45^\circ$ and $\theta = 60^\circ$. The
447 structural response is almost identical to corresponding free field motion in
448 the case of low frequency $f = 1Hz$ and long wavelength 1155m. As the fre-
449 quency increases, structural response is different from free field counterpart
450 because of “base averaging” of “ironing out” effects. This is particularly sig-
451 nificant for high frequency incident wave ($f = 10Hz$) where wavelength is
452 comparable to structural dimension, with observation of significant reduction
453 in structural response. Observed are also wave field disturbance effects in the
454 sense that near field motion is notably altered by the existence of embedded
455 structure, for example, in the case of $f = 10Hz$. Presented examples provide
456 evidence of significance of modeling uncertainties that are introduced by the
457 assumption of uniform, vertically propagating wave field.

458 **5. Acknowledgments**

459 Presented work was supported by the University of California, by private
460 funding sources and in small part by the US-DOE.

461 **References**

- 462 [1] MD Trifunac. A note on rotational components of earthquake motions
463 on ground surface for incident body waves. *International Journal of Soil*
464 *Dynamics and Earthquake Engineering*, 1(1):11–19, 1982.
- 465 [2] MI Todorovska and MD Trifunac. Note on excitation of long structures

- 466 by ground waves. *Journal of Engineering Mechanics*, 116(4):952–964,
467 1990.
- 468 [3] R Betti, AM Abdel-Ghaffar, and AS Niazy. Kinematic soil–structure in-
469 teraction for long-span cable-supported bridges. *Earthquake engineering*
470 *& structural dynamics*, 22(5):415–430, 1993.
- 471 [4] Roman Teisseyre, Takeo Minoru, and Eugeniusz Majewski. *Earthquake*
472 *source asymmetry, structural media and rotation effects*. Springer, 2006.
- 473 [5] Muneo Hori. *Introduction to Computational Earthquake Engineering*.
474 Imperial College Press, 2006. ISBN ISBN-10: 1848163983; ISBN-13:
475 978-1848163980.
- 476 [6] Vlado Gičev, Mihailo D Trifunac, and Nebojša Orbović. Translation,
477 torsion, and wave excitation of a building during soil–structure interac-
478 tion excited by an earthquake SH pulse. *Soil Dynamics and Earthquake*
479 *Engineering*, 77:391–401, 2015.
- 480 [7] JP Wolf. *Dynamic Soil-Structure Interaction*. Prentice-Hall Inc, New
481 Jersey, 1985.
- 482 [8] JE Luco and HL Wong. Response of structures to nonvertically incident
483 seismic waves. *Bulletin of the Seismological Society of America*, 72(1):
484 275–302, 1982.
- 485 [9] MI Todorovska and MD Trifunac. The system damping, the system
486 frequency and the system response peak amplitudes during in-plane
487 building-soil interaction. *Earthquake engineering & structural dynamics*,
488 21(2):127–144, 1992.

- 489 [10] Maria I Todorovska. Effects of the wave passage and the embedment
490 depth for in-plane building-soil interaction. *Soil Dynamics and Earth-*
491 *quake Engineering*, 12(6):343–355, 1993.
- 492 [11] Jianwen Liang, Jia Fu, Maria I. Todorovska, and Mihailo D. Trifunac.
493 Effects of the site dynamic characteristics on soil-structure interaction
494 (i): Incident SH-waves. *Soil Dynamics and Earthquake Engineering*,
495 44(0):27 – 37, 2013. ISSN 0267-7261. doi: 10.1016/j.soildyn.2012.08.
496 013. URL [http://www.sciencedirect.com/science/article/pii/
497 S0267726112002114](http://www.sciencedirect.com/science/article/pii/S0267726112002114).
- 498 [12] Jianwen Liang, Jia Fu, Maria I Todorovska, and Mihailo D Trifunac.
499 Effects of site dynamic characteristics on soil–structure interaction (ii):
500 Incident p and SV waves. *Soil Dynamics and Earthquake Engineering*,
501 51:58–76, 2013.
- 502 [13] AA Stamos and DE Beskos. 3-d seismic response analysis of long lined
503 tunnels in half-space. *Soil Dynamics and Earthquake Engineering*, 15
504 (2):111–118, 1996.
- 505 [14] Vlado Gičev, Mihailo D. Trifunac, and Nebojša Orbović. Two-
506 dimensional translation, rocking, and waves in a building during soil-
507 structure interaction excited by a plane earthquake P-wave pulse.
508 *Soil Dynamics and Earthquake Engineering*, 90:454 – 466, 2016.
509 ISSN 0267-7261. doi: [http://dx.doi.org/10.1016/j.soildyn.2016.01.
510 006](http://dx.doi.org/10.1016/j.soildyn.2016.01.006). URL [http://www.sciencedirect.com/science/article/pii/
511 S0267726116000075](http://www.sciencedirect.com/science/article/pii/S0267726116000075).
- 512 [15] Vlado Gičev, Mihailo D Trifunac, and Nebojša Orbović. Two-
513 dimensional translation, rocking, and waves in a building during soil-

- 514 structure interaction excited by a plane earthquake P-wave pulse. *Soil*
515 *Dynamics and Earthquake Engineering*, 90:454–466, 2016.
- 516 [16] John Lysmer and Roger L. Kuhlemeyer. Finite dynamic model for in-
517 finite media. *Journal of Engineering Mechanics Division, ASCE*, 95
518 (EM4):859–877, 1969.
- 519 [17] Jingbo Liu, Yixin Du, Xiuli Du, Zhenyu Wang, and Jun Wu. 3D viscous-
520 spring artificial boundary in time domain. *Earthquake Engineering and*
521 *Engineering Vibration*, 5(1):93–102, 2006.
- 522 [18] Daniel Baffet, Jacobo Bielak, Dan Givoli, Thomas Hagstrom, and
523 Daniel Rabinovich. Long-time stable high-order absorbing boundary
524 conditions for elastodynamics. *Computer Methods in Applied Me-*
525 *chanics and Engineering*, 241-244(0):20 – 37, 2012. ISSN 0045-7825.
526 doi: <http://dx.doi.org/10.1016/j.cma.2012.05.007>. URL [http://www.](http://www.sciencedirect.com/science/article/pii/S0045782512001557)
527 [sciencedirect.com/science/article/pii/S0045782512001557](http://www.sciencedirect.com/science/article/pii/S0045782512001557).
- 528 [19] Jing-Qi Huang, Xiu-Li Du, Liu Jin, and Mi Zhao. Impact of incident
529 angles of P waves on the dynamic responses of long lined tunnels. *Earth-*
530 *quake Engineering & Structural Dynamics*, 45(15):2435–2454, 2016.
- 531 [20] Jingqi Huang, Mi Zhao, and Xiuli Du. Non-linear seismic responses of
532 tunnels within normal fault ground under obliquely incident P waves.
533 *Tunnelling and Underground Space Technology*, 61:26–39, 2017.
- 534 [21] Xiaowei Wang, Juntao Chen, and Ming Xiao. Seismic responses of an un-
535 derground powerhouse structure subjected to oblique incidence SV and
536 P waves. *Soil Dynamics and Earthquake Engineering*, 119:130 – 143,
537 2019. ISSN 0267-7261. doi: <https://doi.org/10.1016/j.soildyn.2019.01>.

- 538 014. URL [http://www.sciencedirect.com/science/article/pii/](http://www.sciencedirect.com/science/article/pii/S0267726117307935)
539 [S0267726117307935](http://www.sciencedirect.com/science/article/pii/S0267726117307935).
- 540 [22] Dapeng Qiu, Jianyun Chen, and Qiang Xu. Dynamic responses and
541 damage forms analysis of underground large scale frame structures under
542 oblique SV seismic waves. *Soil Dynamics and Earthquake Engineering*,
543 117:216–220, 2019.
- 544 [23] Steven L. Kramer. *Geotechnical Earthquake Engineering*. Prentice Hall,
545 Inc, Upper Saddle River, New Jersey, 1996.
- 546 [24] William T Thomson. Transmission of elastic waves through a stratified
547 solid medium. *Journal of applied Physics*, 21(2):89–93, 1950.
- 548 [25] Norman A Haskell. The dispersion of surface waves on multilayered
549 media. *Bulletin of the seismological Society of America*, 43(1):17–34,
550 1953.
- 551 [26] Jacobo Bielak, Kostas Loukakis, Yoshiaki Hisada, and Chiaki
552 Yoshimura. Domain reduction method for three–dimensional earthquake
553 modeling in localized regions. part I: Theory. *Bulletin of the Seismolog-*
554 *ical Society of America*, 93(2):817–824, 2003.
- 555 [27] George B Arfken and Hans J Weber. *Mathematical methods for physi-*
556 *cists*. AAPT, 1999.
- 557 [28] S Chiriță, C Gales, and ID Ghiba. On spatial behavior of the harmonic
558 vibrations in kelvin-voigt materials. *Journal of Elasticity*, 93(1):81–92,
559 2008.
- 560 [29] Chaiki Yoshimura, Jacobo Bielak, and Yoshiaki Hisada. Domain re-
561 duction method for three–dimensional earthquake modeling in localized

- 562 regions. part II: Verification and examples. *Bulletin of the Seismological*
563 *Society of America*, 93(2):825–840, 2003.
- 564 [30] Jacobo Bielak and Paul Christiano. On the effective seismic input
565 for non-linear soil-structure interaction systems. *Earthquake Engineer-*
566 *ing & Structural Dynamics*, 12(1):107–119, 1984. ISSN 1096-9845.
567 doi: 10.1002/eqe.4290120108. URL [http://dx.doi.org/10.1002/eqe.](http://dx.doi.org/10.1002/eqe.4290120108)
568 [4290120108](http://dx.doi.org/10.1002/eqe.4290120108).
- 569 [31] Marco G. Cremonini, Paul Christiano, and Jacobo Bielak. Implemen-
570 tation of effective seismic input for soil-structure interaction systems.
571 *Earthquake Engineering & Structural Dynamics*, 16(4):615–625, 1988.
572 doi: 10.1002/eqe.4290160411. URL [https://onlinelibrary.wiley.](https://onlinelibrary.wiley.com/doi/abs/10.1002/eqe.4290160411)
573 [com/doi/abs/10.1002/eqe.4290160411](https://onlinelibrary.wiley.com/doi/abs/10.1002/eqe.4290160411).
- 574 [32] J. Enrique Luco. Impedance functions for a rigid foundation on a layered
575 medium. *Nuclear Engineering and Design*, 31:204–217, 1974.
- 576 [33] L. H. Wong and J. Enrique Luco. Tables of impedance functions for
577 square foundations on layered media. *International Journal of Soil Dy-*
578 *namics and Earthquake Engineering*, 4(2):64–81, 1985.
- 579 [34] C. B. Crouse, Behnam Hushmand, J. Enrique Luco, and H. L. Wong.
580 Foundation impedance functions: Theory versus experiment. *Journal of*
581 *Geotechnical Engineering*, 116(3):432–449, March 1990.
- 582 [35] JE Luco. Torsional response of structures for sh waves: the case of hemi-
583 spherical foundations. *Bulletin of the Seismological Society of America*,
584 66(1):109–123, 1976.

- 585 [36] FCP De Barros and JE Luco. Dynamic response of a two-dimensional
586 semi-circular foundation embedded in a layered viscoelastic half-space.
587 *Soil Dynamics and Earthquake Engineering*, 14(1):45–57, 1995.
- 588 [37] JE Luco and HL Wong. Seismic response of foundations embedded in
589 a layered half-space. *Earthquake engineering & structural dynamics*, 15
590 (2):233–247, 1987.
- 591 [38] Jia Fu, Jianwen Liang, and Bin Han. Impedance functions of three-
592 dimensional rectangular foundations embedded in multi-layered half-
593 space. *Soil Dynamics and Earthquake Engineering*, 103:118–122, 2017.
- 594 [39] Boris Jeremić, Zhaohui Yang, Zhao Cheng, Guanzhou Jie, Nima Tafaz-
595 zoli, Matthias Preisig, Panagiota Tasiopoulou, Federico Pisanò, José
596 Abell, Kohei Watanabe, Yuan Feng, Sumeet Kumar Sinha, Fatemah
597 Behbehani, Han Yang, and Hexiang Wang. *Nonlinear Finite Elements:
598 Modeling and Simulation of Earthquakes, Soils, Structures and their In-
599 teraction*. Self Published, University of California, Davis, CA, USA, and
600 Lawrence Berkeley National Laboratory, Berkeley, CA, USA, 1989-2021.
601 ISBN 978-0-692-19875-9. URL: [http://sokocalo.engr.ucdavis.edu/
602 ~jeric/LectureNotes/](http://sokocalo.engr.ucdavis.edu/~jeric/LectureNotes/).
- 603 [40] Hexiang Wang, Han Yang, Sumeet K. Sinha, Yuan Feng, Chao Luo,
604 David B. McCallen, and Boris Jeremić. 3D non-linear earthquake
605 soil-structure interaction modeling of embedded small modular reactor
606 (SMR). In *Proceedings of the 24th International Conference on Struc-
607 tural Mechanics in Reactor Technology (SMiRT 24)*, Busan, South Ko-
608 reas, August 20-25 2017.
- 609 [41] Sumeet K. Sinha, Yuan Feng, Han Yang, Hexiang Wang, Nebojša Or-

- 610 bović, David B. McCallen, and Boris Jeremić. 3-d non-linear modeling
611 and its effects in earthquake soil-structure interaction. In *Proceedings of*
612 *the 24th International Conference on Structural Mechanics in Reactor*
613 *Technology (SMiRT 24)*, Busan, South Korea, August 20-25 2017.
- 614 [42] Boris Jeremić, Guanzhou Jie, Zhao Cheng, Nima Tafazzoli, Panagiota
615 Tasiopoulou, Federico Pisanò, José Antonio Abell, Kohei Watanabe,
616 Yuan Feng, Sumeet Kumar Sinha, Fatemah Behbehani, Han Yang, and
617 Hexiang Wang. *The Real-ESSI Simulator System*. University of Cali-
618 fornia, Davis, 1988-2021. <http://real-essi.us/>.
- 619 [43] W Silva. Body waves in a layered anelastic solid. *Bulletin of the Seis-*
620 *mological Society of America*, 66(5):1539–1554, 1976.
- 621 [44] Kohei Watanabe, Federico Pisanò, and Boris Jeremić. A numerical inves-
622 tigation on discretization effects in seismic wave propagation analyses.
623 *Engineering with Computers*, 33(3):519–545, Jul 2017. ISSN 1435-5663.
624 doi: 10.1007/s00366-016-0488-4. URL [http://dx.doi.org/10.1007/](http://dx.doi.org/10.1007/s00366-016-0488-4)
625 [s00366-016-0488-4](http://dx.doi.org/10.1007/s00366-016-0488-4).
- 626 [45] M Tabatabaie, N Abrahamson, and JP Singh. Effect of seismic wave
627 inclination on structural response. In *Dynamic Response of Structures*,
628 pages 613–620. ASCE, 1986.
- 629 [46] Takahiro Sigaki, Kazuhiko Kiyohara, Yoichi Sono, Dai Kinoshita, Toru
630 Masao, Ryoichi Tamura, Chiaki Yoshimura, and Takeshi Ugata. Esti-
631 mation of earthquake motion incident angle at rock site. In *Proceedings*
632 *of 12th world conference on earthquake engineering*, pages 1–8, 2000.
- 633 [47] Nishant Sharma, Kaustubh Dasgupta, and Arindam Dey. Optimum lat-
634 eral extent of soil domain for dynamic ssi analysis of rc framed buildings

- 635 on pile foundations. *Frontiers of Structural and Civil Engineering*, 14
636 (1):62–81, 2020.
- 637 [48] R. Courant and D. Hilbert. *Methods of Mathematical Physics*. Wiley,
638 1989. ISBN 979-0-471-50447-4.
- 639 [49] Boris Jeremić, Guanzhou Jie, Matthias Preisig, and Nima Tafazzoli.
640 Time domain simulation of soil–foundation–structure interaction in non–
641 uniform soils. *Earthquake Engineering and Structural Dynamics*, 38(5):
642 699–718, 2009.
- 643 [50] Nathan. M. Newmark. A method of computation for structural dynam-
644 ics. *ASCE Journal of the Engineering Mechanics Division*, 85:67–94,
645 July 1959.
- 646 [51] John Argyris and Hans-Peter Mlejnek. *Dynamics of Structures*. North
647 Holland in USA Elsevier, 1991.
- 648 [52] Han Yang, Hexiang Wang, Yuan Feng, Fangbo Wang, and Boris Jeremić.
649 Energy dissipation in solids due to material inelasticity, viscous coupling,
650 and algorithmic damping. *ASCE Journal of Engineering Mechanics*, 145
651 (9), 2019.
- 652 [53] Han Yang, Hexiang Wang, Boris Jeremić, and Jerzy Salamon. Earth-
653 quake soil structure interaction analysis of a gravity dam. In G MAZZA,
654 editor, *Proceedings of the 15th International Benchmark Workshop on*
655 *Numerical Analysis of Dams*. ICOLD, PoLiMi, September 2019.
- 656 [54] José A. Abell, Nebojša Orbović, David B. McCallen, and Boris Jeremić.
657 Earthquake soil structure interaction of nuclear power plants, differences
658 in response to 3-D, 3×1-D, and 1-D excitations. *Earthquake Engineering*

- 659 *and Structural Dynamics*, 47(6):1478–1495, May 2018. doi: 10.1002/eqe.
660 3026. URL [https://onlinelibrary.wiley.com/doi/abs/10.1002/](https://onlinelibrary.wiley.com/doi/abs/10.1002/eqe.3026)
661 [eqe.3026](https://onlinelibrary.wiley.com/doi/abs/10.1002/eqe.3026).
- 662 [55] Keiiti Aki and Paul G. Richards. *Quantitative Seismology*. University
663 Science Books, 2nd edition, 2002.
- 664 [56] Jean-François Semblat and Alain Pecker. *Waves and Vibrations in Soils:*
665 *Earthquakes, Traffic, Shocks, Construction works*. IUSS Press, first edi-
666 tion, 2009. ISBN ISBN-10: 8861980309; ISBN-13: 978-8861980303.
- 667 [57] George W Housner. Interaction of building and ground during an earth-
668 quake. *Bulletin of the Seismological Society of America*, 47(3):179–186,
669 1957.